Annex 3.

Form of opening (renewal) for Project

APPROVED

JINR DIRECTOR

_____/_____

"_____" _____ 2024 г.

PROJECT PROPOSAL FORM

Opening/renewal of a research project/subproject of the large research infrastructure project within the Topical plan of JINR

1. General information on the project

1.1 Theme code: 02-2-1144-2021

1.2 Project code: 02-2-1144-1-2021/2024

1.3 Laboratory: DLNP

1.4 Scientific field: Particle Physics

1.5 Title of the project: Experiment COMET

1.6 Project leader: Tsamalaidze Zviadi

1.7 Project deputy leader:

2. Scientific case and project organization

2.1 Annotation

Charged-lepton flavour-violating (CLFV) processes offer deep probes for new physics with discovery sensitivity to a broad array of new physics models - SUSY, Higgs Doublets, Extra Dimensions, and, particularly, models explaining the neutrino mass hierarchy. The most sensitive exploration of CLFV is provided by experiments that utilize high intensity muon beams to search for CLFV $\mu \rightarrow e$ transitions, such as: $\mu^+ \rightarrow e^+\gamma$ (MEG at PSI, Switzerland); $\mu^+ \rightarrow e^+e^-e^+$ (Mu3e at PSI, Switzerland) and the coherent neutrinoless conversion of a muon into an electron in the field of a nucleus $\mu^-N \rightarrow e^-N$ (COMET at J-PARC, Japan; Mu2e at Fermilab, USA).

COMET experiment [1] will be carried out using a two-staged approach: Phase-I [2] and Phase-II [3].

The experimental sensitivity goal for this process in the Phase-I experiment is 3.1×10^{-15}, or 90% upper limit of branching ratio of 7×10^{-15}, which is a factor of 100 improvement over the existing limit of $B(\mu^- + \mathrm{Au} \rightarrow e^- + \mathrm{Au}) \leq 7\times10^{-13}$ from SINDRUM-II at PSI [4]. The goal of Phase-II is a SES of 2.6×10^{-17}, which is a factor of about 10 000 better than the current experimental limit. The expected

number of background events is 0.032, with a proton beam inter-bunch extinction factor of 3×10^{-11}. To achieve the target sensitivity and background level, the 3.2kW 8 GeV proton beam from J-PARC (Japan) will be used. Two types of detectors: CyDet (the cylindrical detector system) and StrECAL (the straw tracker and the electron calorimeter (ECAL)), will be used for detecting the $\mu^-\rightarrow e^-$ conversion events and for measuring the beam-related background events.

Scientists from DLNP JINR are participating successfully in the preparation stage of the COMET experiment. For Phase-I JINR specialists manufactured and tested all set of straw tubes with a diameter of 9.8 mm and a length of 1.6 m (more than 2700 pieces), and for Phase–II will produce a full set of straw tubes with a diameter of 5 mm. JINR specialists actively participate in the creation of the straw tracker, the electromagnetic calorimeter and a cosmic ray veto system (SRV) at the stages of modeling and scientific and technical works. They will also continue to be actively involved in the assembly and maintenance of these detectors. JINR specialists participate in the analysis of test measurement data and will participate in the analysis of COMET experiment data.

2.2 Scientific case (aim, relevance and scientific novelty, methods and approaches, techniques, expected results, risks)

2.2.1 Physics motivation

Historically, flavour-changing neutral currents have played a significant role in revealing details of the underlying symmetries at the foundation of the Standard Model (SM). In the SM there is no known symmetry that conserves lepton flavour. The discoveries of quark mixing and neutrino mixing, provided profound insights to the underlying physics. Motivated by these past successes, there exists a global programme to explore CLFV processes providing deep, broad probes of Beyond Standard Model (BSM) physics.

The objective is to search for evidence of new physics beyond the SM using CLFV processes in the muon sector. These processes are sensitive to effective new physics mass scales of 10^3-10^4 TeV/c^2, well beyond what can be directly probed at colliders. Over the next few years, currently planned experiments will begin taking data and will extend the sensitivity to CLFV interactions by orders of magnitude. Experimentally, one of the promising process to search for CLFV is direct muon-to-electron conversion via an interaction with a nucleus $\mu^-N \rightarrow e^-N$. The COMET experiment seeks to measure the neutrinoless coherent transition of a muon to an electron ($\mu \rightarrow e$ conversion) in the field of an aluminum nucleus.

The event signature of coherent neutrinoless $\mu^- \rightarrow e^-$ conversion in a muonic atom is the emission of a mono energetic single electron in a defined time interval. The energy of the signal electron for aluminium is 104.97 MeV, and the lifetime of the muonic atom is 864 ns.

This makes neutrinoless $\mu^- \rightarrow e^-$ conversion very attractive experimentally. Firstly, the e^- energy of about 105 MeV is well above the end-point energy of the muon decay spectrum (~52.8 MeV). Secondly, since the event signature is a mono-energetic electron, no coincidence measurement is required. Thirdly, the long lifetime means backgrounds associated with the beam flash can be eliminated. Thus, the search for this process has the potential to improve sensitivity by using a high muon rate without suffering from accidental background events.

Various theoretical models which predict sizable magnitudes of charged lepton mixing branching ratios exist. Among them, most well-motivated models are supersymmetric (SUSY) extension of the SM, such as SUSY-GUT or SUSY-Seesaw models. Also review of the modern theoretical motivations for lepton flavor violation, data from current experimental bounds and expected improvements are collected by Marciano, Mori and Roney [5].

2.2.2 Phase-I

The purpose of COMET Phase-I is two-fold: to make background measurements for Phase-II and to search for μ→e conversion at an intermediate sensitivity. A schematic layout of the COMET experiment is shown in Fig. 1.

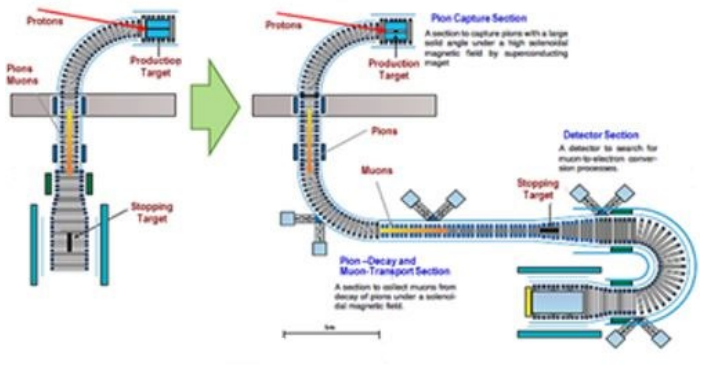

Fig. 1. Schematic layout of COMET Phase-I and COMET Phase-II

The Phase-I will provide a working experience of many of the components to be used in Phase-II and will also produce competitive physics results, both of the μ→e conversion process and of other processes that COMET Phase-II cannot investigate.

The experiment will be carried out in the Nuclear and Particle Physics Experimental Hall (NP Hall) at J-PARC (Japan) using a bunched 8 GeV pulsed proton beam with high inter-bunch extinction factor, that is slow-extracted from the J-PARC Main Ring (MR). Muons for the COMET experiment will be generated from the decay of pions produced by collisions of the 8 GeV proton beam on a production target. The yield of low-momentum muons transported to the experimental area is enhanced using a superconducting pion-capture solenoid surrounding the proton target in the pion-capture section. Muons are momentum- and charge-selected using curved superconducting solenoids in the muon-transport section, before being stopped in an aluminum target. The signal electrons from the muon-stopping target are then transported by additional curved solenoids to the main detector system, including a cylindrical drift chamber (CDC) and the StrECAL detector.

The COMET Phase-I will have the pion-capture and the muon-transport sections up to the end of the first 90° bend of the full experiment (Fig. 2). The muons will then be stopped in the aluminum target at the center of a cylindrical drift chamber in a 1T magnetic field.

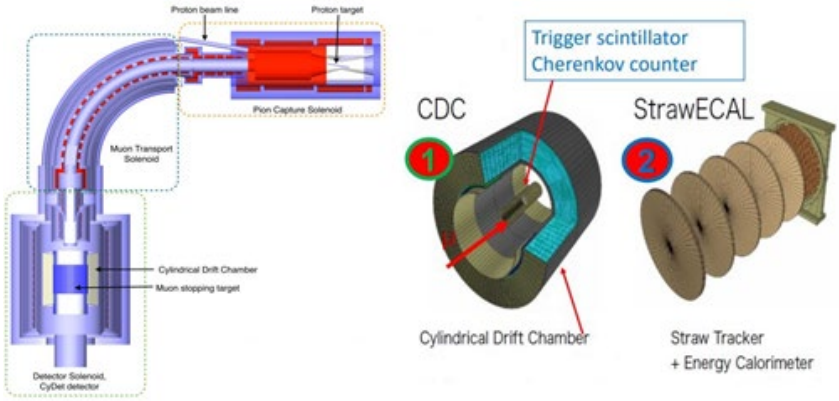

Fig. 2. Schematic layout of the COMET Phase-I setup

The experimental setup for Phase-I will be augmented with prototypes of the Phase-II StrECAL detector.

For Phase-I a total number of protons on target of 3.2×10^{19} is planned which will provide around 1.5×10^{16} muons stopped in the target. This will enable the design goal of COMET Phase-I to be achieved: a SES, which, in the absence of a signal, translates to a 90% confidence level branching ratio limit of 7×10^{-15}.

Physics Sensitivity for Phase-I

COMET will operate in CyDet mode to search for μ→e conversion in Phase-I. The SES for a given number of stopped muons, is determined by:

$$B(\mu^- + Al \rightarrow e^- + Al) = \frac{1}{N_\mu \cdot f_{cap} \cdot f_{gnd} \cdot A_{\mu-e}} \qquad (1)$$

where N_μ is the number of muons stopped in the target. The fraction of captured muons to total muons on target $f_{cap} = 0.61$ is taken, while the fraction of μ→e conversion to the ground state in the final state of $f_{gnd} = 0.9$ is taken [6]. $A_{\mu\text{-}e} = 0.041$ is the net signal acceptance. To achieve SES of 3×10^{-15}, $N_\mu = 1.5\times10^{16}$ is needed. By using the muon yield per proton of 4.7×10^{-4} a total number of protons on target of 3.2×10^{19} is needed. With a proton beam current of 0.4 μA, the measurement requires about 146 days although there are considerable uncertainties such as the pion production yield.

Other searches

In contrast to COMET Phase-II, the CyDet detector surrounds the muon stopping target directly in Phase-I, and can observe both positive and negative particles from the muon stopping target. This allows for a search for the lepton-number-violating process $\mu^-N\rightarrow e^+N$ ($\mu^-\rightarrow e^+$ conversion) concurrently with the $\mu^-N\rightarrow e^-N$ search. The anticipated experimental sensitivity for $\mu^-\rightarrow e^+$conversion could be similar to $\mu^-N\rightarrow e^-N$ conversion, although a detailed estimation has not yet been performed. In addition, the cylindrical drift chamber will have a relatively large geometrical coverage, and thereby a coincidence measurement with a large solid angle is achievable. This allows a search for $\mu^-e^-\rightarrow e^-e^-$ conversion in a muonic atom, which is an as-yet unmeasured process. Using a lower-intensity beam ($<10^7$ muon/s) a measurement of $\mu^-e^-\rightarrow e^-e^-$could be carried out with the CyDet detector.

2.2.3 Background measurements

While the signal of $\mu^-N\rightarrow e^-N$ is 105 MeV mono-energetic electron, there are several potential sources of electron background events in the energy region around 100 MeV, which can be grouped into three categories as follows: intrinsic physics backgrounds, which come from muons stopped in the target; beam-related backgrounds; other miscellaneous backgrounds due to cosmic-rays.

Phase-I will be used to obtain data-driven estimates of backgrounds, and hence inform the detailed design of COMET Phase-II. In Phase-I the StrECAL detector will be placed at the downstream end of the muon-transport beam line and will be dedicated to background measurements, in particular: direct measurement of the inter-bunch extinction factor, direct measurement of unwanted secondary particles in the beam line such as pions, neutrons, antiprotons, photons and electrons, direct measurement of background processes that have not been measured at the required accuracy, such as muon decays in orbit (DIO) and radiative muon capture (RMC).

2.2.4 Phase-II

This final stage includes creating a full beam line, using a higher beam intensity and changing the detector configuration. The main detectors for the $\mu^-\rightarrow e^-$ conversion search will be straw tracker and ECAL. These modifications, together with experience gained during Phase-I, will make possible to

carry out a search for $\mu^- \rightarrow e^-$ conversion at the SES of 3×10^{-17} [3]. A comparison of the Phase-I and Phase-II parameters is given in Table 1.

Table 1. COMET Phase-I and Phase-II parameters

Parameter	Phase-I	Phase-II
Beam power	3.2 kW (8 GeV)	56 kW (8 GeV)
Running time	150 days	1 year
Proton beam target material	graphite	tungsten
#protons on target	3.2×10^{19}	8.5×10^{20}
#muon stops (N_μ)	1.3×10^{16}	2.0×10^{18}
Muon rate/s	5.8×10^{9}	1.0×10^{11}
#muon stops/proton	0.00052	0.00052
#background events	0.032	0.34
The detector acceptance ($A_{\mu\text{-}e}$)	0.06	0.04
SES	3.1×10^{-15}	2.6×10^{-17}
Upper limit (90% C.L.)	$< 7 \times 10^{-15}$	$< 6.0 \times 10^{-17}$
Planned start of measurements	2025-2026	2028-2029

2.2.5 COMET requirements

Highly intense muon source

To achieve an experimental sensitivity better than 10^{-16}, O(10^{18}) muons are needed. Two methods are adopted to increase the muon beam intensity. One is to use a high-power proton beam from J-PARC, the other is to use a highly efficient pion collection system. The latter is achieved by surrounding the proton target with a 5T superconducting solenoid. The principle of this pion-capture system has been experimentally demonstrated at the MuSIC (Muon Science Innovative beam Channel) facility at Research Centre for Nuclear Physics (RCNP), Osaka University [7].

Proton beam pulsing with high proton extinction

In order to suppress the occurrence of prompt beam-related background events, a pulsed proton beam will be employed, where proton leakage between the pulses is tightly controlled. As a muon in an aluminum muonic atom has a lifetime of the order of 1 μs, a pulsed beam can be used to eliminate prompt beam background events by performing measurements in a delayed time window, provided that the beam pulses are shorter than this lifetime and the spacing between them is comparable or longer. Stringent requirements on the beam extinction, defined as the number of leakage protons with respect to the number of protons in a beam pulse, are necessary. Tuning of the proton beam in the MR, and using extinction-improving techniques, extinction factor at level 10^{-11} is achieved.

Curved solenoids for charge and momentum selection

High momentum muons can produce electron background events in the energy region of 100 MeV, and therefore must be eliminated. This is achieved by transporting the pion/muon beam through a system of curved superconducting solenoids. As they pass through the curved solenoid, the centres of the helical motion of the charged particles drift perpendicularly to the plane in which their paths are curved, with the magnitude of the drift proportional to their momentum. To compensate for this a dipole field parallel to the drift direction will be applied for a given reference momentum to keep the centres of the helical trajectories in the bending plane. Hence, with suitably placed collimators, high momentum and positively charged particles can be eliminated. Since the muon momentum dispersion is proportional to a total bending angle, the COMET C-shape beam line produces a larger separation of the

muon tracks as a function of momentum and hence an improved momentum selection. In COMET Phase-II, additional curved solenoids will be used in a C-shaped electron transport system between the muon-stopping target and the electron spectrometer to eliminate low-momentum backgrounds to the electron signal.

Pion production at the primary target

The proton target will be installed within the bore of the capture solenoid and designed to maximise the capture of low-energy negative pions produced in the backward direction. Both the target station and muon-capture solenoid region will be designed for the Phase-II beam power of 56 kW since once constructed and exposed to the beam, the target station infrastructure will be activated, and cannot be modified. However, the target itself will be replaced between the two phases, and the target station will be designed with remote handling capability to allow for this.

While pion production is maximised with a high-Z material, it is proposed to use a graphite target for Phase-I. This will minimise the activation of the target station and heat shield, which will significantly ease the necessary upgrades for Phase-II operation where a tungsten target will be employed.

The Phase-I beam power of 3.2 kW will deposit a heat load of approximately 100 W in the graphite target material. This can easily be radiated to the solenoid shield. The target support system to accurately position the target within the solenoid inner shield will have a low-mass design. The choice of proton energy was determined by considering the pion production yield and backgrounds. In particular, backgrounds from antiproton production are important. The current choice of proton energy is 8 GeV, which is above the threshold energy for antiproton production (6.56 GeV).

Pion capture

The pions are captured using a high-strength solenoidal magnetic field giving a large solid angle acceptance. The pion-capture system consists of the pion production target, high-field solenoid magnets and a radiation shield. Pions emitted into the backward hemisphere with a transverse momentum less than 100 MeV/c are captured by using a solenoid magnet field of 5 T. This gives adequate acceptance for the parent pions of muons with momentum below 75 MeV/c.

Muon beam transport

The muon beam transport consists of curved and straight superconducting solenoid magnets of 3 T and ~7.6 m long. The requirements are:

● the muon transport should be long enough for pions to decay to muons (for instance, for about 20 m, the pion survival rate for pions with the reference momentum is about 2×10^{-3});

● the muon transport should select muons with low momentum (~40 MeV/c) and eliminate muons of high momentum (>75 MeV/c) to avoid backgrounds from muon decays in flight, since their decays in flight would produce spurious signals of ~105 MeV electrons.

The optimal muon momentum is ~ 40 MeV/c. Muons with higher momentum are less likely to be stopped and give rise to backgrounds in the signal region from decays in flight. Positive muons are another potential source of background. Curved solenoid transport is used to minimise these.

To keep the centre of the helical trajectories of the 40 MeV/c muons in the bending plane, the COMET Phase-I beam line uses one curved solenoid with a bending angle of 90° with a compensating dipole field of ~0.05 T. The collimator system is designed to remove particles travelling 8.5 cm above or 10 cm below the beam height and will be realised by installing two plates of stainless steel at the exit of the muon-transport system. To separate the muon stopping target region, filled with helium, from the

muon beam line in vacuum, a vacuum window of 500 μm titanium will be installed at the exit of the curved solenoid. The muon-transport section and the detector solenoid (DS) are connected by the beam bridge solenoid (BS), where the magnetic field changes from 3 T to 1 T.

Muon beam yields

Estimates using the QGSP_BERT model of the number of muons and pions per proton after the muon-transport section and on the muon stopping target are summarised in Table 2. With a 0.4 μA proton beam, the yield of stopped muons is about 1.2×10^{9} per second.

Table 2. Muon and pion yields per proton after the BS and stopped in the muon stopping target

Yield (per proton)	After muon-transport section	Stopped in muon target
Muons	5.0×10^{-3}	4.7×10^{-4}
Pions	3.5×10^{-4}	3.0×10^{-6}

Muon-stopping target

The muon-stopping target is placed in the center of the DS and designed to maximize the muon stopping efficiency and acceptance for the $\mu^{-}\rightarrow e^{-}$ conversion electrons. The design must also minimize the energy loss of the conversion electrons as this increases their momentum spread.

To eliminate beam-related background events the measurement window will only open approximately 0.7 μs after the primary proton pulse.

High-Z materials are not appropriate for the stopping target since the muonic atom lifetime decreases with increasing Z, therefore aluminum (Z = 13) with a muonic atom lifetime of 864 ns was chosen.

The target consists of 17 aluminum flat disks, 100 mm radius and 200 μm in thickness, with 50 mm spacings [8].

2.2.6 Detector system

During Phase-I running, CyDet, detector system StrECAL and cosmic ray veto (CRV) system will be used.

The primary purpose of StrECAL in Phase-I is to make direct measurements of the composition of the muon beam and backgrounds, but the detector system is very similar to the detectors, which will be employed in Phase-II, and act as a prototype for the Phase-II detectors.

2.2.6.1 CyDet

The cylindrical detector system is the main detector system for the $\mu^{-}\rightarrow e^{-}$ conversion search in Phase-I. It consists of a cylindrical drift chamber (CDC) and a cylindrical trigger hodoscope (CTH). Fig. 3 shows a schematic layout of the CyDet. It is located after the BS in the muon transport section, and installed inside a large superconducting DS, with a magnetic field of 1 T, and around the stopping target.

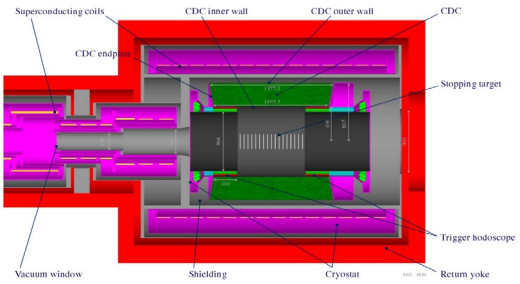

Fig. 3. Schematic layout of the CyDet detector

This detector has been adopted for Phase-I as there is no downstream curved solenoid electron transport and so most beam particles that do not stop in the muon-stopping target will go downstream and escape from the detector region without leaving any hits in the detector system.

A key feature of COMET is to use a pulsed beam that allows for the elimination of prompt beam backgrounds by looking only at tracks that arrive several hundred nanoseconds after the prompt beam flash.

The main parameters of the CDC are summarised in Table 3. The radii of the inner and the outer walls are chosen to avoid electrons from muon decays in orbit (DIO) with momentum less than 60 MeV/c from hitting the CDC and to fully cover the tracks of 105 MeV/c signal electrons. The walls are made from carbon fibre reinforced plastic (CFRP). The inner and outer walls have thin aluminium foils glued inside them to eliminate charge-up on the CFRP. The endplates are conical and about 10 mm thick. Trigger hodoscopes are placed at both the upstream and downstream ends of the CDC.

The detector is designed to avoid high hit rates due to beam particles, DIO electrons and low-energy protons emitted after the nuclear capture of muons. Among the small fraction of particles, which eventually enter the CDC and leave hits, DIO electrons and low energy protons dominate. The protons are easily identified, because the energy deposits in the CDC cells are about 100 times larger than that of similar-momentum electrons. To achieve the required sensitivity for Phase-I, the momentum resolution must be about 200 keV/c for 105 MeV electrons. At this energy, the momentum resolution is dominated by multiple-scattering. Consequently, the CDC must be a low-mass detector and this dictates its design and the choice of the gas mixture.

Table 3. Main parameters of the CDC

		Length (mm)	Radius (mm)	Thickness (mm)
Inner wall		1495.5	496.0-496.5	0.5
Outer wall		1577.3	835.0-840.0	5.0
Number of sense layers		20 (including 2 guard layers)		
	Material	Diameter (μm)	Number of wires	Tension (g)
Sense wire	Au-plated W	25	4986	50
Field wire	Al	126	14562	80
	Mixture		Volume (L)	
Gas	He:i-C_4H_{10} (90:10)		2084	

2.2.6.2 Straw tracker

Since the momentum of the electrons from $\mu^- \rightarrow e^-$ conversion is as low as 105 MeV/c, the intrinsic momentum resolution is dominated by multiple scattering of electrons in the tracker material. Therefore, reduction of a total mass of the tracking detector and placing it in a vacuum environment are of great importance. For these requirements, a straw-tube gas wire chamber technology has been selected for the tracker.

In Phase-I the straw tracker will make direct measurements of the particles in the muon beam line, and the rate of particle production (in particular anti-protons), as a function of beam energy and other backgrounds. It will be placed inside the vacuum vessel and the DS, which has a field strength of 0.8−1.1 T. The detector will provide a precise measurement of a particle's momentum and its identity, through dE/dx, E/p and the time of flight information in combination with the calorimeter. For Phase-I, as shown in Fig. 4, many kinds of particles will reach and enter the DS.

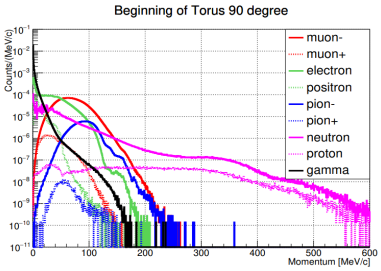

Fig. 4. Momentum distributions of various beam particles at the exit of the first 90° curved solenoid, using a graphite proton target

Overall structure

The overall structure of the straw tracker is schematically shown in Fig. 5. Each of the five tracker super-layers, called «stations», consists of four planes: two to measure the x coordinate and two to measure the y coordinate. Each pair of planes is staggered by half a straw diameter in order to solve left-right ambiguities. Each station is constructed as a stand-alone unit and mounted on the detector frame, which is inserted and removed from the DS on rails and linear bearings. The gas mixture is suppplied into the straw tubes from the gas system through the end-plugs, which are glued into the straws and in which the anode wires are fixed. The anode wires are held at high voltage and the straw wall is grounded, to act as the cathode. The straws have a diameter of 9.8 mm and 5 mm for Phase-I and Phase-II, respectively. The station is made of aluminum and has a round shape, so the length of the tubes varies from 692 mm to 1300 mm.

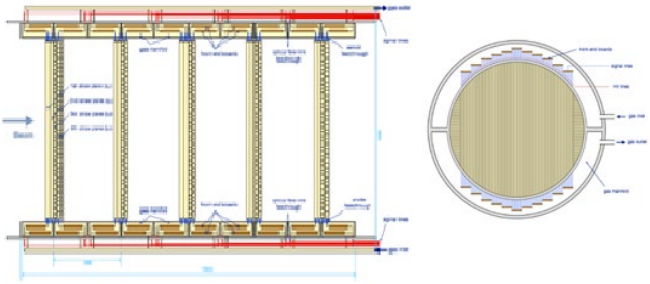

Fig. 5. Schematic view of the straw tracker (the straw dimensions are scaled by a factor of three for clarity): (left) side view; (right) cross-sectional view of a plane

Straw tubes

Thin-walled drift tubes are manufactured by ultrasonic welding with an oscillation frequency of 44 KHz. For Phase-I the wall thickness of the straw is 20 μm, and the diameter is 9.8 mm, for Phase-II - 12 μm and 5 mm. The 9.8 mm diameter tubes were produced in JINR LHEP at the facility set up for the NA62 [9]. For the production of 5 mm diameter straw using the ultrasonic welding technology of the NA62 group, a room of the 6th class of cleanness with constant control of temperature within 22-23ºC (±0.1ºC) and humidity of 43-44% (±10%) was equipped in JINR DLNP, and the SRP-STRAW facility was designed and created. The main difference between SRP-STRAW and NA62 facility is the use of a fixed gap between hammer and anvil. The tubes are made of pre-cut mylar film with a thickness of 20 μm or 12 μm and with an aluminum coating with a thickness of 70 nm, the width of the cut depends on the final diameter of the straw: 9.8±0.02 mm and 5±0.02 mm. Reducing the straw wall thickness from 20 to 12 μm provides a reduction in multiple scattering, and reducing the tube diameter from 9.8 to 5 mm improves the detector loading characteristics. The seam width of the straw is approximately 500 μm. The SRP-STRAW machine (Fig. 6) is equipped with an automatic welding process control system. Strict quality control for mechanical deformations, using laser and by supercharging the straw

is carried out at each production stage. Production of 5 mm diameter straw has been started (Fig. 7). The results of checking 9.8 mm straw seam for strength are shown in Fig. 8, the diameter stability of 5 mm straw along the length is shown in Fig. 9.

Fig. 6. General view of the SRP-STRAW machine

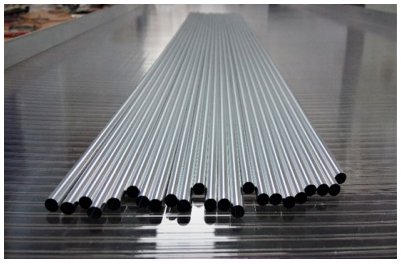

Fig. 7. Tubes with diameter of 5 mm and wall thickness of 12 μm

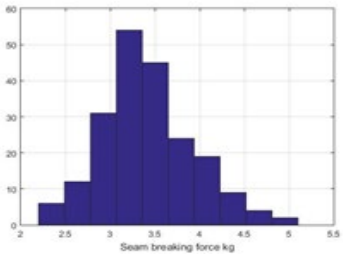

Fig. 8. Seam strength of 9.8 mm straw

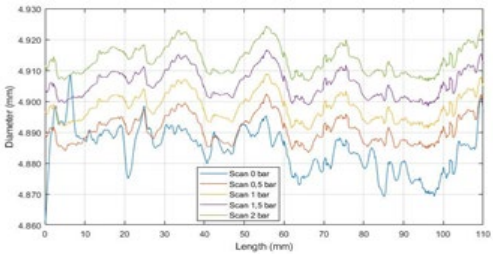

Fig. 9. Straw diameter scan at different pressures

Gas mixture

The Phase-I gas mixture is Ar:C_2H_6 (50:50). Due to the good drift properties of this mixture, such as a small Lorentz angle in the magnetic field, a small diffusion coefficient and a constant drift velocity, good spatial resolution can be achieved. In a magnetic field of 1 T, the Lorentz angle is ~45° at an electric field strength of 1 kV/cm, and ~20° - at 4 kV/cm. The radial drift velocity is expected to be 5 cm/μs at 1 kV/cm, and 4.5 cm/μs at 4 kV/cm, giving a resolution of ~150 μm. For Phase-II, other options for gas mixtures are also being considered, for example, Ar:CO_2 (70:30).

Study of the mechanical properties of straw tubes

Straw tubes with a diameter of 9.8 mm produced at JINR were tested, and possible deformations of the straw as a function of the pre-tensioning value were investigated. The measurement results of sag (defined by the deformation made by gravity from the normal position without gravity) and elongation for 1 m straw are shown in Fig. 10.

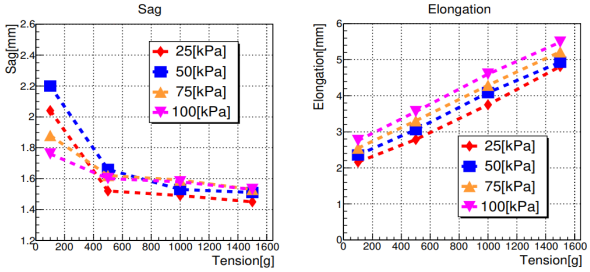

Fig. 10. Straw-pre-tensioning study results; (left) the sag that is found for various pressure differences across the straw wall as a function of applied tension, (right) elongations of the straws

Research shows that tension higher than 1 kg_F prevents sagging, and this results in an elongation of 1.7-2.0 mm. Therefore, straw deformation can be avoided by stretching the straw by 2 mm during assembly.

The sense wires are chosen to be gold-plated tungsten containing 3% rhenium. Additional supports for the anode wires are not required. Assuming a straw radius of 4.9 mm, an anode wire radius of 12.5 μm, a capacitance/length of 10.5 pF/m, a maximum voltage of 2.2 kV, and a critical length of 2 m, the required tension on the wire is found to be approximately 70 g.

For straw, it is also important to consider the relaxation process associated with a decrease in tension over time [10]. This process is usually called tension relaxation. To study the relaxation process, the JINR-COMET group created a stand (Fig. 11), which provides control of humidity, temperature and straw tension during measurements [11].

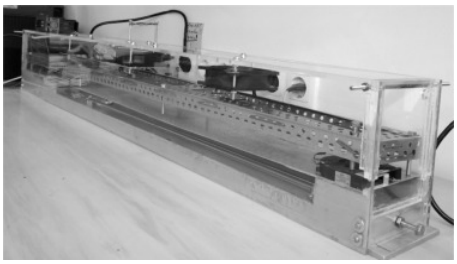

Fig. 11. General view of the stand

The relaxation process is well described by an exponential relationship with two constants:

$$T = 0.29 \cdot e^{-\frac{t}{0.23}} + 0.30 \cdot e^{\frac{-t}{7.0}} + 15. \quad (2)$$

Fig. 12 illustrates the process of relaxation over a long period of time. After a period of time 3T2, the action of the exponential terms of the tension attenuation ceases and the tension begins to fall according to a linear law with a slope of 0.0035 N/day. The dependence of tension relaxation in time makes it possible to assess the performance of the straw detector in the experiment. Taking into account the initial tension T_0 = 15.6 N, the tension relaxation includes an exponential fall in the interval of 210 days and a linear fall in the tension interval of (0.72–0.25)T_0. Based on the above estimates, the service life of the straw will be (210 days + (0.72–0.25)/0.0035) = 6.5 years, which is sufficient for Phase-I COMET.

The dependence of straw stress on strain was also measured [10] (Fig. 13). Up to the value of the straw stress of 30×10^6 N/m^2, the linear dependence is preserved, the deformation is plastic and obeys Hooke's law [12, 13], which corresponds to a tension of 1850±1 gf. It follows that the upper limit of the straw tension can be increased to ~1.9 kgf.

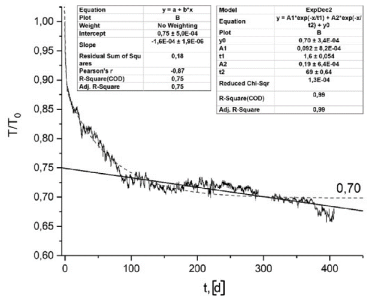

Fig. 12. Tension relaxation over a long period of time

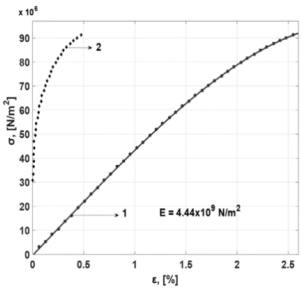

Fig. 13. Stress dependence on straw strain (X-axis – tension, Y-axis – elongation), (1) – interpolation of experimental data, elastic deformation region, (2) – plastic deformation

Currently, the 5 mm diameter tension relaxation test bench is being upgraded.

Straw tracker readout electronics

The electron track generates about 50–60 electron-ion pairs in the straw tube. In order for the analog signal supplied to the ROESTI input stage to be ~480 fC , a gas gain of ~5×10^4 is required. About 10% of this charge is collected in 6 ns. To set the discriminator threshold at approximately 16 fC or two

primary electrons, a pre-amplification of the signal of ~1 V/pC is necessary. To achieve the required momentum resolution (<200 keV/c) in a straw tracker, the spatial resolution in the straw must be ~150 μm. Given the drift velocity in the straw, the readout electronics require a time resolution of ~2 ns and high radiation hardness. The total number of readout channels is about 5 thousand, so power consumption must be strictly limited, and the physical dimensions of the detector impose restrictions on the linear dimensions of the readout electronics. The schematic diagram of the ROESTI (Read Out Electronics for Straw Tube Instrument) board is shown in Fig. 14.

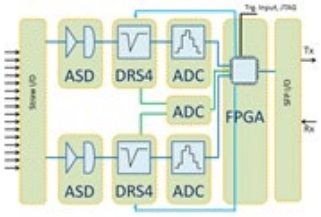

Fig. 14. Schematic diagram of the ROESTI board

The main parameter that determines the performance of the readout electronics is the time resolution. When test signals are applied to the input of the ROESTI board, the time resolution is 160 ps, which is sufficient for track reconstruction (Fig. 15).

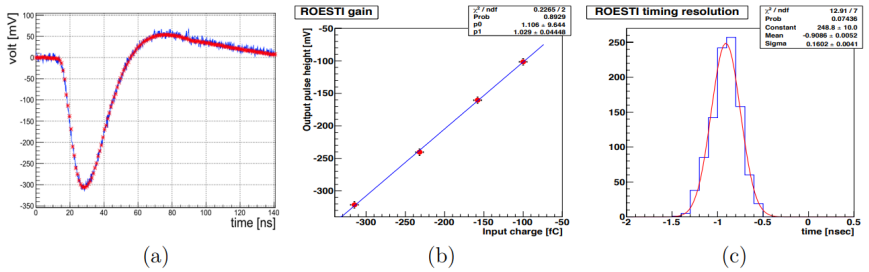

(a) (b) (c)

Fig. 15. ROESTI board parameters: (a) test pulse output, (b) gain calibration, (c) time resolution

Prototype with single 9.8 mm straw channel

The single straw prototype was built to investigate gas leakage during operation in vacuum (Fig. 16).

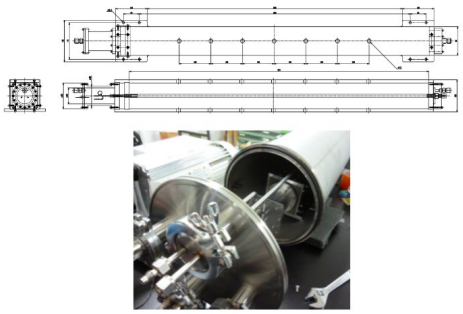

Fig. 16. Single straw prototype: (top) prototype drawing; (bottom) general view of the stand

Leak-tightness measurements revealed a leak rate of 0.0035 cm^3/min per meter of straw (Fig. 17), which, when scaled to the full straw tracker, is well within the acceptable level to keep required gas pumping rate.

The results of the study of a single-channel prototype confirm the possibility of using straw with wall thickness of 20 μm manufactured by ultrasonic welding for Phase-I COMET.

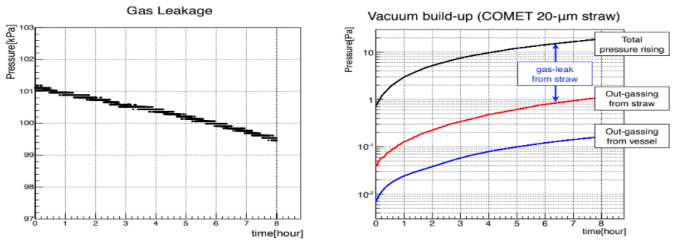

Fig. 17. Measured gas leakage: (left) pressure drop inside the straw over time with initial pressure of 2 bar; (right) pressure increase over time after pump closure

Full-scale prototype of a tracker station with 9.8 mm straw

At Tohoku University Research Center (ELPH, Research Center for Electron Photon Science Tohoku University), Japan, a full-scale prototype was tested using an electron beam with pulses of 50-300 MeV/c, Fig. 18 shows the scheme and general view of the experimental setup.

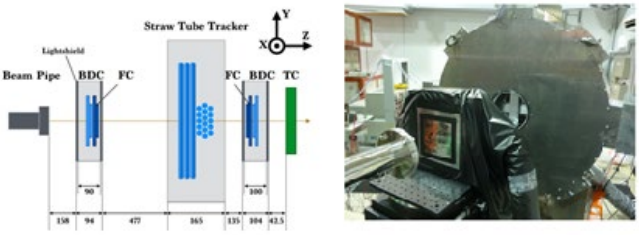

Fig. 18. Experimental setup for testing the tracker and calorimeter prototypes: (left) schematic view of the setup, (right) view of the setup from the incoming beam side

BDC (Beam-Defining Counter) is a counter for determining the trajectory of beam particles by their coordinates in the chambers, which consists of mutually perpendicular rows of optical scintillating fibers of FC (Finger Counters) with a thickness of 1 mm. The trigger signal is generated by the coincidence of signals from the FC and TC (Timing Counter), which consists of a plastic scintillator with high light output and a fast PMT with a fine grid to ensure accurate time measurement. Fig. 19 shows the measured detection efficiency of a single straw tube for a gas mixture Ar:C_2H_6 (50:50) depending on the applied high voltage. From the graph in Fig. 19 it can be seen that voltage above 1800 V guarantees the maximum possible efficiency for a single straw, although gaps between straws in the station can lead to a slight loss of efficiency.

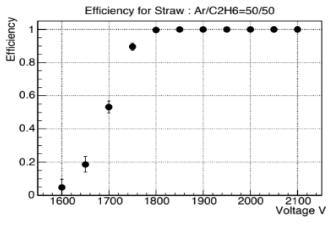

Fig. 19. Single straw detection efficiency

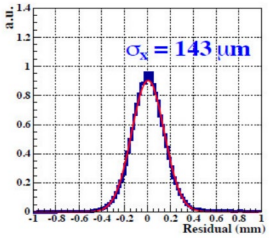

Fig. 20. Evaluation of the tracker station prototype spatial resolution

Fig. 20 shows the obtained spatial resolution of ~143.2 μm for the track (gas mixture Ar:C_2H_6 (50:50), HV 1900 V). Taking into account inaccuracy in determining the point of entry and exit of the beam, the spatial resolution of the station can be estimated as ~119.3 μm.

The left plot of Fig. 21 shows the measured dependence of spatial resolution on track position for Ar:C_2H_6 (50:50) and HV of 2000 V, and the right plot - the spatial resolution simulated with GARFIELD++: the green graph shows the ideal spatial resolution, thus it can be seen that the spatial resolution dependence on electron track position is well-reproduced in simulation.

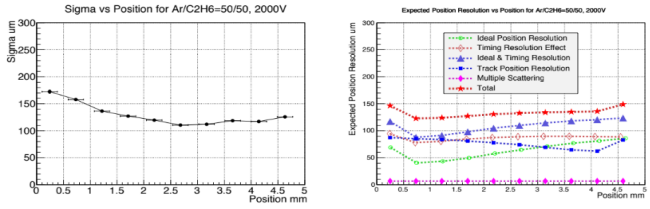

Fig. 21. Spatial resolution dependence on track position: (left) measured, (right) simulated

At J-PARC, the straw tracker stations for Phase-I COMET are being assembled (Fig. 22): one station is completely ready, electronics are being installed on the second station, and it is planned to complete 4 stations by the end of the year. JINR COMET employees are taking part in the assembly of the second station.

Fig. 22. Assembly of a tracker station for Phase-I

Prototype with a single 5 mm straw channel

A single-channel prototype (5 mm diameter and 50 cm length straw) was created in JINR SRP to study the electrical parameters of the straw. Measurements were carried out with Ar:CO_2 (60:40) gas mixture, at 1680 V, with Fe^{55}+Co^{57} radioactive sources, Fig. 23 shows the obtained energy spectrum. The measurement results allow to conclude that the tube operates in proportional mode, the gas gain is estimated to be ~10^4. Thus, it was shown that 5 mm straw tubes produced at the SRP-STRAW facility can be used in the track system of the COMET detector.

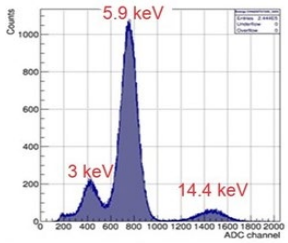

Fig. 23. Spectrum obtained on a single-channel prototype (5 mm straw)

Mini prototype of a tracker module with 5 mm straw

At DLNP JINR the assembly of a straw tracker prototype with 32 tubes along the X axis and 32 tubes along the Y axis has begun. The tubes have a diameter of 5 mm, a wall thickness of 12 μm and a length of 50 cm. The work on the prototype allows to develop a technology for assembling and fastening 5 mm tubes in tracker stations for Phase-II (Fig. 24).

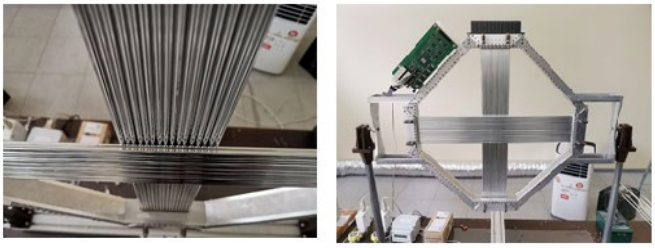

Fig. 24. Assembly of a 64-channel mini prototype of straw tracker module

After completing the assembly and testing the performance of the channels of the mini prototype, it is planned to measure the spatial resolution on the beam of the Linac-200 electron accelerator (DLNP, JINR). Further, the prototype will be sent to the Research Center of Tohoku University (Japan).

JINR pilot version of the straw tracker module

At the COMET collaboration technical board, it was decided to develop and manufacture at JINR a pilot version of the straw tracker module, consisting of 5 mm straw. Achieving this goal requires solving a number of tasks:

- development and production of the module's frame (Fig. 25);
- production of 5 mm straw tubes;
- development and production of all components of end-plugs for straw tubes;
- modification and production of the ROESTI board;
- development and creation of a ROESTI board cooling system;
- development and creation of a system for supplying gas mixture to straw;
- development and creation of an equipment for the assembly of the module.

Currently, the work is at an intermediate stage, where some components have already been developed and produced (the module's frame, partially the ROESTI boards), and some (end-plugs components, etc.) have been developed and will be manufactured or purchased.

The most difficult and time-consuming part was the development and production of the frame for the module. It should be noted that the production of such a product is a high-tech process due to the huge number of precision milling and drilling to a great depth, with need to maintain the wall thickness between adjacent holes of 0.5 mm (Fig. 26). This requires precision machines with a large base for product placement and capable of moving the working part in 6 spatial coordinates. We managed to find a company with such equipment, and they manufactured the frame of the module.

Fig. 25. Straw module frame

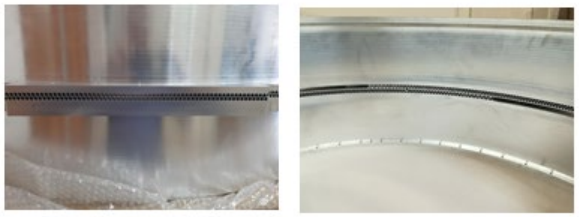

Fig. 26. Hole spacing

The module frame has the following parameters:

- the diameter after assembly is 1610 mm;
- the number of straws inserted into the frame is 936 (468 along X + 468 along Y);
- the diameter of each hole in the frame is 5 mm;
- the distance between holes in one row is 0.5 mm;
- the distance between adjacent rows is 0.5 mm;
- the distance between rows X and Y is 5 mm;
- there are 4 prefabricated gas distribution blocks for supplying the gas mixture to the straw (Fig. 27).

The design of the frame is prefabricated, the gas distribution blocks are attached to the frame once all the tubes have been assembled in it. This design allows access to the straw tubes during assembly and separates the flow of the working gas, entering the chambers of the gas distribution system units, from the cooling gas, that flows through the enclosed space of the module containing the ROESTI boards.

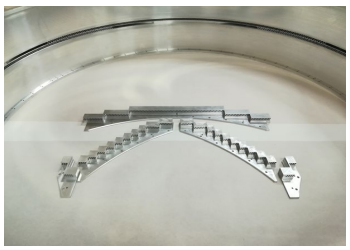

Fig. 27. Gas distribution block

There were no ready-to-use ROESTI boards, but the documentation for them was provided by Japanese developers. A number of modifications were made to adapt them to local production conditions and to improve some of their operating conditions. Of the 60 boards required for module operation, 25 were manufactured and tested (Fig. 28).

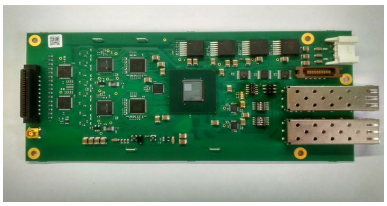

Fig. 28. Manufactured ROESTI board

The module assembly procedure is quite complicated and cannot be implemented without a special equipment, that ensures the fixation of the frame and its rotation around the X and Z coordinates (Fig. 29).

The prefabricated design of the end-plugs (2 parts: 3.5 mm and 5 mm in diameter; Fig. 30) allows to insert the inflated tubes into the frame and then stretch them. A part of the end-plug with a diameter of 5 mm is glued into the tube, and a 3.5 mm part, with a hole for passing the working mixture into the straw tube, passes through a gas distribution block.

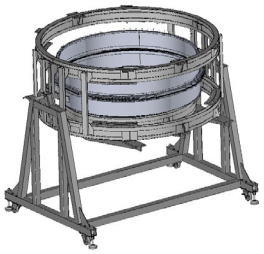

Fig. 29. Equipment for assembling a module with a frame inside

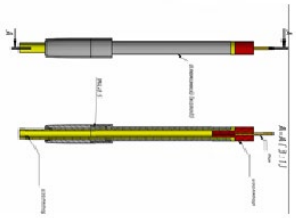

Fig. 30. Prefabricated design of end-plug

The gas system for the straw and the gas cooling system for the boards have been developed, and some components of these systems have been purchased.

2.2.6.3. Electromagnetic calorimeter

Calorimeter

A fundamental feature of the COMET experiment is the large angles of incidence of recorded electrons on the end surface of the segmented electromagnetic calorimeter (ECAL) cells, because ECAL is located in a uniform magnetic field. The main task of the ECAL is to measure the released energy when registering a 105 MeV electron with an accuracy sufficient to reliably separating it from background events. The ECAL of the COMET experiment must have an energy resolution of no worse than 5% and a spatial resolution of no worse than 1 cm to reduce the influence of the background from DIO on the recorded signal events lying in the narrow energy region of 105±0.5 MeV. The ECAL must

solve the following problems: 1) measure the electron energy with high accuracy; 2) reliably separate electrons, neutrons and low-energy gamma quanta [2].

For the ECAL of the COMET experiment were selected the scintillation single crystals based on lutetium oxyorthosilicate doped with cerium (LYSO:Ce). Parameters of these crystals best satisfy the requirements of the experiment, namely, crystals have high density (7.1 g/cm^3), high light yield (~32000 photon/MeV), fast decay time (~41 ns), which significantly expands the range of their application [14-17].

At present, in experimental physics, there are still no experiments where these crystals would be used [18]. The main factor limiting the use of these crystals in this field is their high price, as well as a number of disadvantages. A significant disadvantage of LYSO:Ce crystals is a considerable variation of the light yield both over the length of an individual crystal (in the growing direction) and for different crystals, that will lead to an error in measuring the energy released in the calorimeter and deterioration of the energy resolution [19-21].

The creation of the ECAL requires solving some problems. First, the simulation of the calorimeter optimal structure is needed. Secondly, it is necessary to study the influence of the light yield variation in crystals and the non-uniformity of the light yield along the length on the accuracy of the measured released energy in the calorimeter, i.e. on the amount of uncertainty in the detector response. Thirdly, it is required the development of methods and algorithms for improving the uniformity of the detector response associated with the non-uniformity of light collection along the crystal length. In addition, there is the task of the measuring of the non-uniformity of the response of the ECAL prototype using cosmic muons at different angles (0^o, 9^o and 19^o) of particle incidence relative to the end surface of the crystals.

Measurements of the non-uniformity of the light yield distribution along the LYSO:Ce crystal length by gamma spectroscopy were performed on a precision setup. Basic elements of the setup are a mechanical system, data acquisition system, a high-speed measuring system based on the VX1742B digitizer [22] with a frequency of 5 GHz and a high-speed trigger system on NIM blocks. The mechanical system is capable to establish the position of the source with an accuracy of 1 μm. Data acquisition system consists of two fast low-noise photomultipliers (Hamamatsu H1949-51), located at both ends of the crystal [23] and performing correlation measurements of the crystal parameters. The setup is fully automated.

Using gamma spectroscopy method it was calibrated (uniformity, light collection loss along the crystal length, relative light yield) 50 LYSO:Ce crystals from Saint-Gobain Crystals Inc. (S-G) with dimensions of 20×20×120 mm^3, which were then used in the ECAL prototype for measurements in the Beam Test (2014, March, 10-19, Tohoku, Japan). Calibration was carried out for crystals without wrapper. The relative light yield was measured under the same conditions. The calibrated ^{22}Na radiation source was located in the collimator at a height of 12 mm above the sample, at a distance of 60 mm from the PMT. Fig. 31 presents the results of the relative light yield measuring of these crystals.

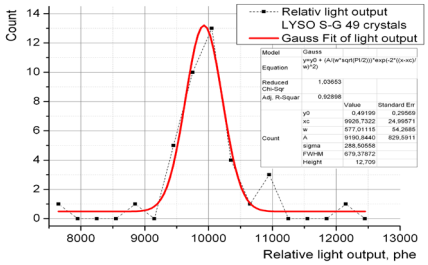

Fig. 31. Relative light yield distribution for 50 S-G LYSO:Ce crystals

The analysis of the results of this distribution gives a light yield variation ~30% [24], and mean value of the LYSO:Ce energy resolution (FWHM) is 8.9%, the non-uniformity coefficient

is ~ 1.2%/cm^{-1} [25]. Thus, when creating the ECAL, it is necessary to select the crystals with similar light yield in ECAL modules.

The main problem in obtaining the required ECAL energy resolution in the COMET experiment is related to the non-uniformity of the light yield of LYSO:Ce crystals, both along the length and within the volume of the scintillator. Many defects (electron traps), which affect the variation of the scintillation properties along the length and perimeter of the crystal, are formed in the crystal structure, when crystals are grown using the Czochralski method. Therefore, Saint-Gobain has developed LYSO:Ce,Ca and LYSO:Ce,Mg crystals with additional doping with Ca and Mg ions, which significantly reduces the efficiency of electron traps, which leads to a more uniform distribution of light yield along the length and volume of the crystal. For example, double-doped LYSO:Ce,Ca crystals have slightly better parameters (light output is 20% higher, energy resolution ~6.5%, decay time - 40 ns). The COMET collaboration has about 60 such crystals at its disposal, and the task arose to study the optical properties of this crystal and compare it with the LYSO:Ce crystal.

S-G LYSO:Ce crystals were studied, namely: 8 samples of LYSO:Ce, which were randomly selected from a batch of 300 units, and 8 samples of LYSO:Ce,Ca, also randomly selected from a batch of 60 units. The samples had dimensions of 20×20×120 mm^3. The samples under study were wrapped with reflective tape of 65 μm thick (TEFLON AF2400). The crystals were measured on a precision measuring setup by gamma spectroscopy method. A calibrated ^{22}Na radiation source was installed in a lead collimator (thickness of 3 mm and aperture diameter of 0.5 mm), which was located at a distance of 12 mm above the crystal surface. Measurements were carried out in 5 mm increments.

As a result of the investigations were obtained that the mean value of the scintillator response non-uniformity for LYSO:Ce crystals is ~4.6% (Fig. 32), while for LYSO:Ce,Ca crystals it is ~1.1%. It was found that for the group of LYSO:Ce crystals under study, the energy resolution variation at the middle of the length is ±0.21%, and for LYSO:Ce,Ca (Fig. 33) it is ±0.19%. The light yield variation near the end surface of the crystals is approximately 26% and 20% for LYSO:Ce and LYSO:Ce,Ca, respectively. The response time of LYSO:Ce crystals is 8 ns longer than that of LYSO:Ce,Ca.

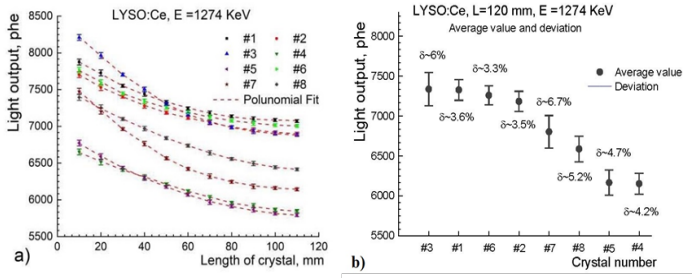

Fig. 32. a) Light yield non-uniformity along the LYSO:Ce crystal length; b) Scintillator response non-uniformity measured at an energy of 1274 keV

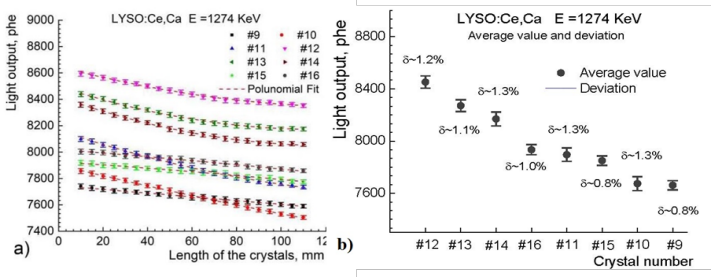

Fig. 33. a) Light yield non-uniformity along the LYSO:Ce,Ca crystal length; b) Scintillator response non-uniformity measured at an energy of 1274 keV

The main result of these studies is for LYSO:Ce crystals the scintillator response non-uniformity is equals approximately 4 times more than for LYSO:Ce,Ca. However, it should be noted that both types of crystals make it possible to create a detector that meets the requirements of the COMET experiment. Nevertheless, LYSO:Ce,Ca crystals will be more suitable for the COMET experiment calorimeter, allowing to measure the energy released in the calorimeter with an error approximately 4 times smaller than for the case of using LYSO:Ce crystals [26].

Since, ECAL will be located in a uniform electromagnetic field, all electromagnetic showers will be non-paraxial, and will intersect at different angles a number of active (crystal) and passive (wrapper) cells of the calorimeter. In this case, to reduce the measurement error of the released energy in ECAL, it is necessary to solve the following problems: 1) reduce the electromagnetic shower losses in the crystal wrapping materials; 2) eliminate optical cross interference between the neighboring calorimeter cells; 3) improve light collection in the calorimeter cells by reducing losses of the emission of the optical photons.

These problems can be solved by proper selection of the reflective wrapping materials and wrapping method. In the case of LYSO:Ce crystals, the wrapper must be thin, create a diffuse surface, be transparent to electromagnetic shower, and at the same time trap optical photons inside the crystal, preventing optical cross interference. Such materials can be Teflon (AF1601) and ESR tape (VM2000). Fig. 34 presents the results of a study of the light yield non-uniformity for various types of the reflective materials [27].

The best results were obtained with combined-type wrapper, namely: two layers are Teflon (internal) and one layer is ESR (external). Fig. 35 shows the LYSO:Ce crystal energy spectrum obtained for optimal wrapper. The energy resolution for a crystal with optimal wrapper is 8.4 and 8% for energies of 1.173 and 1.332 MeV, respectively [20].

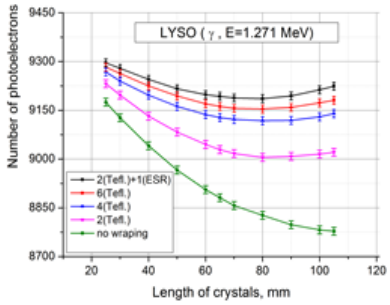

Fig. 34. Light yield non-uniformity along the crystal length with various types of wrapping materials

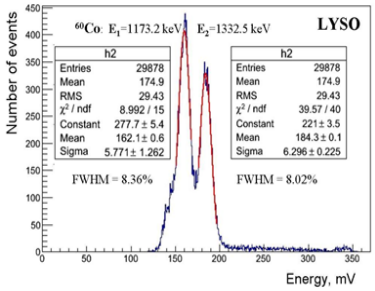

Fig. 35. Energy spectrum obtained with the ^{60}Co source for LYSO crystal wrapped by 2Teflon+ESR

To measure the ECAL response non-uniformity at different angles of incidence of the particles on the end surface of the calorimeter, the optical parameters of the ECAL prototype on LYSO:Ce crystals were measured using cosmic muons at angles of incidence of particles 0°, 9° and 19° relative to the end surface of the crystals. S-G LYSO:Ce crystals [14] were used as scintillators in measurements. Each crystal was wrapped with two layers of Teflon AF1601 (65 μm thick, with an absorption coefficient of 41%/cm), one layer of ESR VM2000 tape (65 μm thick, with reflecting coefficient of 0.99/0.1) and one layer of black paper (200 μm thick).

The ECAL prototype (Fig. 36) consisted of 4 LYSO:Ce crystals with dimensions of 120 × 20 × 20 mm^3. For the light collection from the crystals was used Hamamatsu PMT H1949-51. The PMTs were mounted on the end face of the crystal using optical grease (OKEN6262A, Oken, Japan).

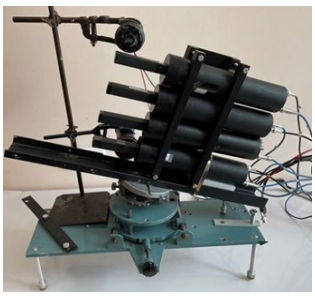

Fig. 36. COMET calorimeter prototype

The trigger counter was made on plastic with dimensions of 10×20×1 mm^3, and the PMT Hamamatsu E2183-500 was used for the light collection [23]. The counters were located at a distance of 256 mm one above the other, and the effective overlap area was S_{eff} = 10×5 mm^2. To measure signals from the PMT, a 32-channel 5 GHz digitizer VX1742B was used [22].

Thus, the detector response non-uniformity depends on the angle of incidence of cosmic muons relative to the end surface of the ECAL prototype. The mean values and non-uniformities of the scintillator response by angle are presented in Fig. 37. The ECAL prototype resolution estimate gives 6% for 19°, 2% for 9° and 4% for 0° [28, 29].

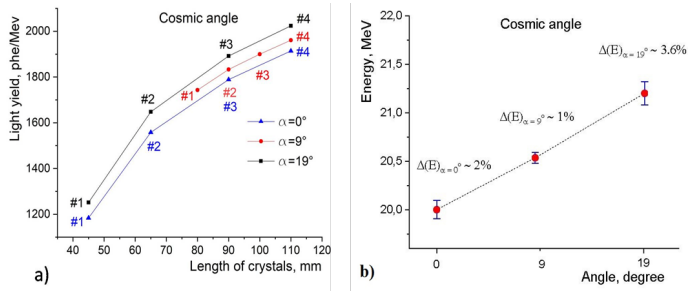

Fig. 37. Non-uniformity of the detector response for the angles of 0°, 9° and 19° measured using cosmic muons a) distributions of the scintillator responses non-uniformity of the calorimeter prototype on the angle; b) mean values and non-uniformity of the detector response on the angle

In the future, it is planned to study the parameters of the ECAL prototype using the electron beam of the Linac-200 accelerator (DLNP, JINR).

As a result of the conducted scientific and methodological research and measurements, the following conclusions can be drawn:

- when creating a calorimeter, it is necessary to select crystals with similar optical parameters in ECAL modules;
- when assembling the ECAL, it is necessary to use reflective wrapping materials and the method of their wrapping, which will improve light collection in the calorimeter cells, reduce the loss of electromagnetic shower in the wrapping materials and eliminate cross interference between the neighboring calorimeter cells;
- the calorimeter response non-uniformity is associated with the physical properties of LYSO:Ce crystals, which depends on the angles of incidence of particles on the end surface of the calorimeter and will affect the energy resolution. This problem cannot be solved physically. Its solution requires the use of special algorithms and offline processing methods [20].

Assembling cell modules and studying parameters of the ECAL prototype

The basic unit of the ECAL is a 2×2 crystal matrix module, with 480 modules to cover the full cross-section of the detector region. A prototype module without a preamplifier is shown in Fig. 38. Each crystal is wrapped with two layers of 76 μm thick high reflection Teflon tape. One Hamamatsu

S8664-1010 APD [30] is attached to each crystal, using a transparent 2 mm thick silicon rubber (ELJEN Technology, EJ-560) as an optical contact between the crystal and the APD (Fig. 39 (a)). This crystal structure was then wrapped in 20 μm thick Mylar (Fig. 39 (b)). This module has been successfully tested at the electron beam accelerator of Tohoku University. The modules are further arranged to form a super-module (Fig. 39 (c)).

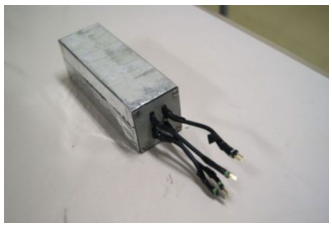

Fig. 38. Crystal module without preamp board

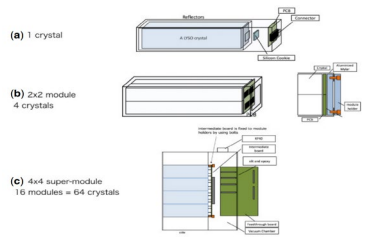

Fig. 39. ECAL modular structure: (a) 1 crystal + 1 APD; (b) 2×2 crystals module; (c) super module 4×4 (64 crystals) and readout system

The checking and calibration of 50 S-G LYSO [24] and GSO crystals were given. The first ECAL prototype was tested in a 65–145 MeV/c electron beam at Tohoku University in March 2014. Each prototype consisted of 49 GSO crystals (matrix 7×7 crystals, with crystal dimensions 20×20×150 mm^3) and S-G LYSO:Ce (matrix 7×7 crystals, with crystal dimensions 20×20×120 mm^3), 7 preamplifier boards and electronics prototype with APD Hamamatsu S8664-55 with an active area of 5×5 mm^2. The prototypes were installed inside the vacuum chamber together with the intermediate board and the feedthrough board. The vacuum chamber was designed to evaluate the parameters of the ECAL prototypes under real-life conditions.

The energy resolution was obtained by converting the signal from each of the 49 crystals using a clustering algorithm. Fig. 40 shows the energy spectra of ECAL prototypes on GSO and LYSO:Ce crystals using an electron beam of 105 MeV/c.

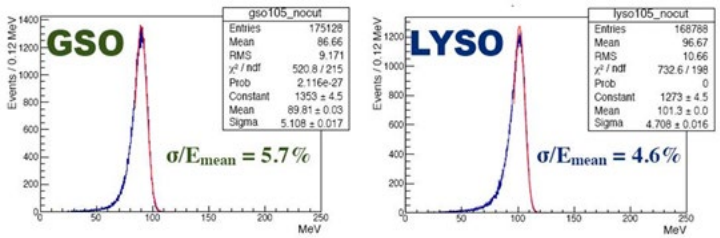

Fig. 40. Energy spectra of prototypes at 105 MeV/s electron beam

Fig. 41 shows the energy resolution as a function of beam energy. The resolution at 105 MeV/c was 5.70 ± 0.02 (stat) ± 0.04 (syst) % for GSO and 4.60 ± 0.01 (stat) ± 0.07 (syst) % for LYSO:Ce. The LYSO crystals are found to meet the required energy resolution of better than 5 % at 105 MeV energy. These measurements also confirmed that LYSO:Ce crystals meet the spatial resolution requirement (1 cm). In addition, based on the measurement results, the collaboration selected the LYSO:Ce crystal.

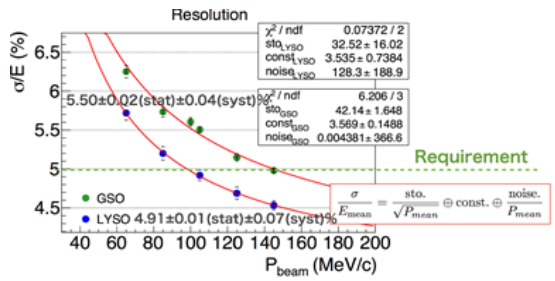

Fig. 41. The measured energy resolution as a function of beam momentum

In December 2015, the ECAL prototype on LYSO:Ce crystals (8×8 matrix) was tested at the electron accelerator beam with an energy of 65–145 MeV/c at Tohoku University. The results are consistent with the results of the 2014 Beam Test, and the energy resolution of the ECAL prototype was 4.2%, indicating that the LYSO:Ce crystals meet the ECAL requirements of the COMET experiment.

2.2.6.4 Cosmic-Ray Veto

The CRV system is one of the most important components of the COMET experiment. Its purpose is to detect cosmic muons with an efficiency of at least 99.99% to identify them during data collection. Subsequently, events involving them should be excluded from the general analysis, to achieve the SES level of 10^{-17}.

Active protection is provided by the cosmic ray muons (CRM) detection system covering the CyDet area. Detailed studies of the background caused by cosmic rays show that the Bridge solenoid (BS) region should also be covered by CRV since CRM in the BS can produce electrons that scatter off the BS, enter CDC and CTH, and simulate signal events. A CRM background suppression factor of at least 10^4 is required, and it is obtained by offline analysis and identification of CRM events in the CRV. The active veto system covering CyDet consists of scintillator-based detectors (Scintillator CRV), whereas cameras with resistive plates made of glass (GRPC) are provided in the BS region.

CRV system based on scintillation strips (SCRV)

The JINR COMET group is a leader in the R&D, design and development of the SCRV system. This activity includes two parts: the completion of the SCRV design, which includes provision for the production of scintillation strips, tests, and a schedule for CRV module manufacture; and the design/creation/testing of electronics embedded in scintillators.

We designed and manufactured the first module of the scintillation strip subsystem of the COMET CRV system – the so-called SCRV-LS-0 module. It consists of four layers of strips, 16 strips in each layer, with aluminum sheets separating these layers and suppressing gamma and beta radiation.

Fig. 42 shows the principle of particle registration and the general design of a single SCRV channel. A single scintillation strip has a cross-sectional area of 0.7×5 cm^2 and a length of up to 420 cm. It is made of polystyrene (Styron 143E) acting as an ionization and photon carrier medium with 2% scintillating fluors (p-terphenyl) and 0.05% POPOP.

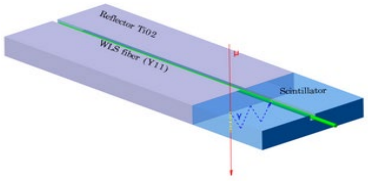

Fig. 42. Sketch of the design for a single channel and the principles of particle detection

Wavelength-shifted fibers (WLS) are used for a CRV strip readout, which transmits light to photodetectors. WLS fibers are necessary to compensate for scintillator short attenuation lengths and optically connect scintillators to photodetectors. A WLS fiber is placed along the strip length in a surface groove.

Many studies have been conducted to optimize the light collection from strips, refine their geometry, and increase the number of optical fibers up to 2 to achieve a compromise between the maximum value of the light collection from a strip and its uniformity across the strip. Also, using GEANT4, various values of the thickness of aluminum plates between the layers of a module and the shift magnitude between layers were studied.

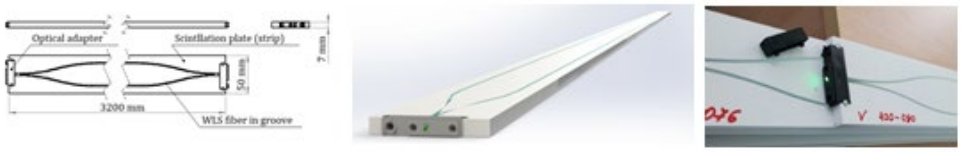

Fig. 43. Strip design and photo of one end of a real strip

Our research has shown that the SCRV module design, consisting of 4 layers of 16 plastic scintillation strips in each layer with a cross-section of 7×50 mm^2 and two WLS fibers with a diameter of 1.2 mm (for side modules: CRV Left and CRV Right) and 1.4 mm (for upper modules - CRV Top), glued into grooves along the strips, should provide the required efficiency of up to 99.99% for the registration of cosmic muons (Fig. 43). Light is collected by Hamamatsu MPPC/SiPM S14160-3050HS. A design of PCB for SiPM has also been developed (Fig. 44).

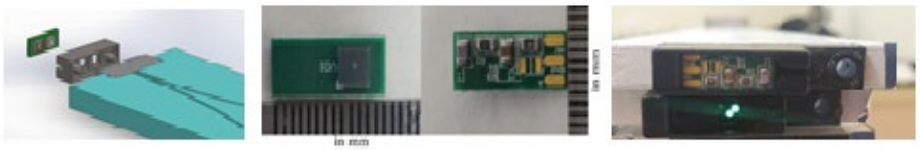

Fig. 44. Design drawing of the connection between photodetector and strip;
Hamamatsu MPPC/SiPM 14160-3050HS photodetector, soldered to the board and placed by the strip

The strip and CRV module final designs were discussed at the 34th and 35th COMET collaboration meetings and approved for SCRV-LS-0.

SCRV module: design, simulation, and calculations

Module simulations were conducted to select the module design, the optimal thickness of aluminum plates suppressing background events was selected, and additional neutron shielding was chosen.

CRV module effectiveness simulation: theoretical foundations of the module effectiveness calculating

For simulation, it is necessary to calculate the probability of particle registration individually for each strip. The probability of registering a particle on one strip, taking into account light collection (μ) and discrimination at the level of $T_{ph.e.} = 5$ photoelectrons, is calculated using formula (3):

$$P(\mu) = \frac{1}{2} + \frac{erf\left(\frac{(\mu - T_{ph.e.})}{\sqrt{2}\mu}\right)}{2} \quad (3)$$

Then, the efficiencies of the strips lying in one layer are combined to obtain the total probability of particle registration by the layer according to formula (4):

$$P_L = 1 - \overline{P_L} = 1 - \prod_{i=1}^{N}\left(1 - P_{S_i}\right) \quad (4)$$

The coincidence of any 3 of the 4 layers creates the overall probability of detecting a particle for the CRV module, which is calculated using formula (5):

$$P_m = \sum_{n=0}^{3} P_{L(i\%4)} P_{L((i+1)\%4)} P_{L((i+2)\%4)} (1 - P_{L((i+3)\%4)}) + P_{L0} P_{L1} P_{L2} P_{L3} \quad (5)$$

Simulation should take into account the technological gaps between the active areas of the strips, the distance between the layers, and the shift of one layer relative to another (**Fig. 45**). A set of such shifts makes up the so-called pattern. It was necessary to determine the effectiveness of more than 64 thousand patterns in order to find the most optimal one. Each pattern includes more than 60 thousand tracks with different directions and entry points into the module: the position "0 mm" is in the middle of

the 8th strip of the upper module; the angle "0 degrees" corresponds to the vertical; the area from -40 mm to +40 mm (red area) was sorted in 0.1 mm increments; and the angle varied from -75 to +75 degrees in increments of 1 degree (orange lines) at each position from -40 to +40 mm (Fig. 45). To significantly reduce the calculation time, we have developed a simplified method for calculating light collection.

Fig. 45. Module pattern, technological gaps. Illustration of the muon track from -75 to 75 degrees of inclination and from -40 to +40 mm away from the central upper strip

According to the simplified model, first, the distribution of the light collection across the strip is found using a transverse scan of the strip. Then, this distribution is used to calculate the light collection according to the track direction and the charged particle flight area (Fig. 46). The light collection is calculated for the muon track by summing the light charges in each mini-section using the formula (6):

$$\mu = \int F_{\mu}(y)dy \approx \sum \mu_i l_i \qquad (6)$$

Here, μ_i is the average light collection per millimeter inside the selected area between the two dotted lines, and l_i is the length of a muon track within this area.

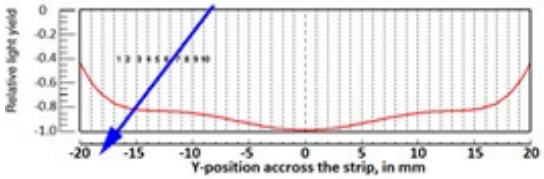

Fig. 46. Simplified light collection calculation model (blue arrow - muon track, red curve -$F_{\mu}(y)$ distribution of light collection by the width of the strip)

The comparison of different module designs with varying geometries of strip utilizing a single WLS fiber or a pair of it showed that the most optimal strip geometry is a 7×50 mm^2 strip with two WLS fibers in parallel grooves at a distance of 30 mm from each other (Table 4).

Table 4. Comparison of the effectiveness of two modules composed of strips with widths of 40 and 50 mm

Aluminum sheets thickness (mm)	Efficiency for the module with 40 mm wide strip and pattern 9-7-7		Efficiency for the module with 50 mm wide strip and pattern 9-7-7		Comment
	For 21 ph.e.	For 25 ph.e.	For 21 ph.e.	For 25 ph.e.	The gap between neighbor strips is 100 μm for all cases
2	0.9998 95	0.9999 92	0.9999 24	0.9999 99	
10	0.9996 22	0.9999 25	0.9998 67	0.9999 81	

The COMET collaboration has approved our proposal for the Top CRV modules with a length of 4.2 m to use two fibers with a diameter of 1.4 mm and two grooves spaced 30 mm apart to achieve the best light collection. For CRV Left/Right modules with a length of 3.2 m, could be used 1.2 mm fibers inserted into two grooves with a 30 mm distance between them. A comparison of efficiency under the same conditions reveals that a strip with a width of 50 mm is preferable to the one with a width of 40 mm. However, background noise increases slightly when the strip's width increases from 40 mm to 50 mm.

Estimated radiation background

Calculations show that the CRV system of the COMET experiment will experience a significant radiation load from neutrons, gamma quanta, and associated electrons (Table 5).

Table 5. Radiation load from neutrons and gamma quanta

	Neutron fluence for 100 days, n/cm^2	Gamma fluence for 100 days, γ/cm^2	Neutron's rate per strip per second per cm^2	Gamma's rate per strip per second per cm^2	Estimation of detection on the threshold at 170 keV for neutrons per second per cm^2	Estimation of detection on the threshold at 170 keV for gammas per second per cm^2
Top	6.6E9	11.7E9	7.6E2	13.5E2	**46**	**26**
Left side	7.4E9	11.1E9	8.6E2	12.8E2	**52**	**24**
Right side	9.5E9	19.2E9	10.9E2	22.2E2	**66**	**42**

It became necessary to calculate the thickness of the aluminum plates between the layers in the module, as well as the additional combined protection (30% boron polystyrene 10 mm thick and lead sheet 5 mm thick) from neutrons and electrons by installing it in front of the module (Fig. 47).

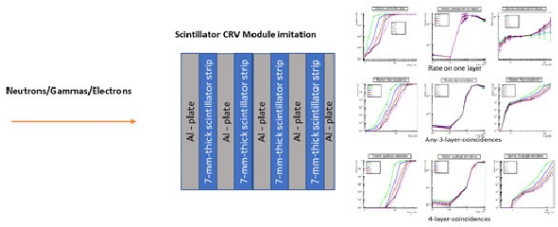

Fig. 47. Radiation loads on the module at different thicknesses of the aluminum sheet between the layers; their weakening depending on the thickness of the aluminum sheets

The simulation conditions were as follows: the discrimination level was set to 170 keV, which corresponds to a 5 ph.e. threshold level with a light collection of 35 ph.e for a strip with a thickness of 7 mm. To simplify the calculations, a 1000×1000 mm square module was created in GEANT4, consisting of 4 layers of scintillator and layered with aluminum sheets. The particles entered the center of the module (Fig. 48). Based on this simulation, the COMET collaboration adopted the following set of aluminum sheets for the CRV module: the 1st base layer - 10 mm aluminum sheet; the 2nd, 3rd and 4th – 5 mm; the 5th top layer – 2 mm.

We also investigated the background loads when adding a combined shield of 30% boron polystyrene with a thickness of 10 mm and a 5 mm lead sheet.

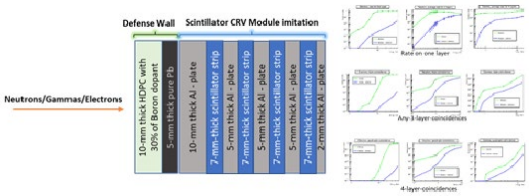

Fig. 48. Additional shield and attenuation of radiation load depending on the thickness of aluminum sheets

Creation of front-end electronics for CRV modules

Two R&D projects for CRV Front-End-Board electronics (FEBE) are currently underway (Fig. 49). They include the development of a prototype of FEBE on «Meteor-32» (INP SB RAS, Novosibirsk) based on «Meteor-8», FEBE (JINR, Dubna) based on the well-known ROC-like family of ASIC

microchips, currently PetiROC chips, prototyping of FEBE for GRPC has also begun. The JINR COMET group has already made a proposal to try using the AST-1-1 ASIC chip (developed by the Institute of Nuclear Problems of the Belarusian State University), and a prototype board with 32 channels using this ASIC in pair with Altera Cyclone 10 has already been created, and its tests are conducted. Together with colleagues from the Budker Institute of Nuclear Physics SB RAS (Novosibirsk), we have developed a form factor and the main functionality to design the FEBE (Fig. 50).

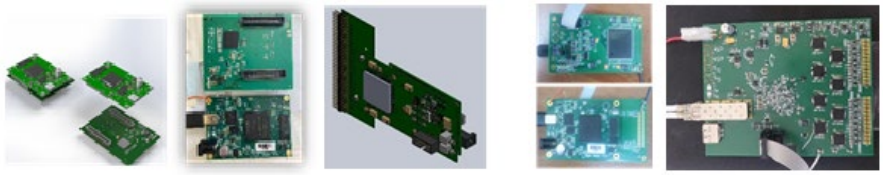

Fig. 49. Development of front-end electronics based on CITIROC, PETIROC, AST-1-1

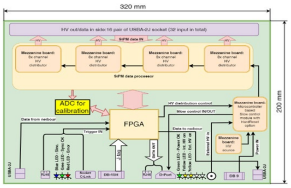

Fig. 50. The first version of FEBE, agreed upon with colleagues from Novosibirsk

Preparation for the production of CRV modules

For the production of the first module, it was decided to produce 100 strips with a length of 3.2 m and a cross-section of 7×50 mm^2, with two grooves, and the Kuraray Y11 WLS fiber with a diameter of 1.2 mm glued in each. These counters were manufactured by «Uniplast» (Vladimir). It has been found that these fibers sometimes have inhomogeneities or damage along their length. It was necessary to check them BEFORE gluing them into the grooves to reduce defects. The fiber quality control procedure was supposed to be simple and fast to be performed by the staff. A stand and a verification procedure satisfying these conditions were created (Fig. 51). The blue light is produced in the scintillator illuminated by UV diodes. This light was then captured by a WLS fiber. Hamamatsu S12571-100C MPPC is placed at the end of the fiber and operates in current generation mode (aka “solar panel”), and the photocurrent from SiPM is registered using a 5-bit FLUKE 187 multi-meter. The photocurrent is measured at 20, 110, 170, 260, and 320 cm distances. In this way, colleagues from «Uniplast» measured fibers to manufacture 100 strips. The 14 fibers out of 214 were found to be defective and were discarded.

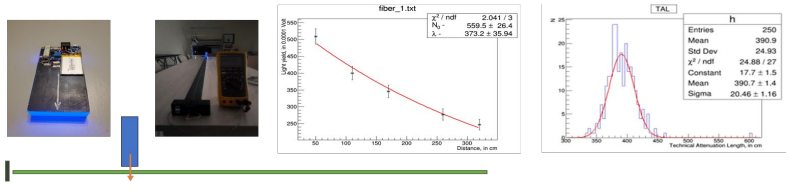

Fig. 51. A blue light source; a light source at a distance of 320 cm from the photodetector; the attenuation length of one of the fibers; distribution of attenuation lengths

After manufacturing the strips, their light collection will be studied at JINR for further selection when creating the module. For this purpose, a measuring stand has been developed to measure 16 strips using a beta-radioactive source simultaneously. We designed a «black box» with a 2D-portal inside (Fig. 52). The length of the box is 6 m, and the width is 1.2 m. Access is provided from all sides. A 2D-portal installed inside the box moves the beta-source along the length and width of the table. Portal control is integrated into the overall data acquisition system.

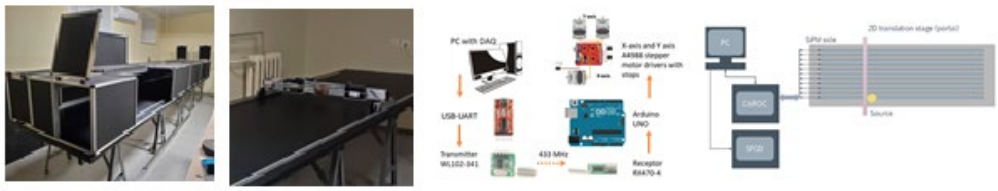

Fig. 52. «Black box» with a 2D-portal inside; 2D-portal on a table; block-diagram of wireless control of 2D-portal for moving a beta-source; block diagram of front-end electronics

Production of the first module

A module assembly technology was developed to create the first module with a length of 3.2 m, consisting of 64 strips made by «Uniplast», with 4 layers each of 16 strips, layered with aluminum sheets. For this, we created a special stand that ensures the necessary compression of the module during gluing with a pressure of 1 atm by vacuuming to fix the geometry while glue curing (Fig. 53). This is equivalent to compressing the module by approximately 26 tons.

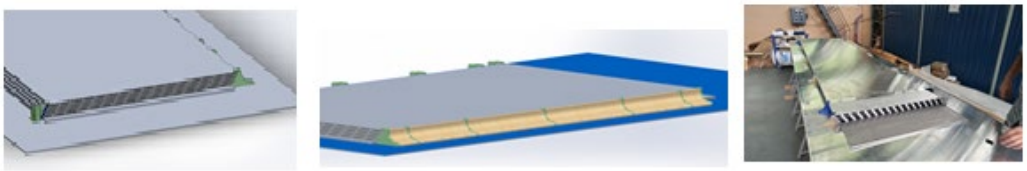

Fig. 53. Design of the assembly table; smooth wooden inserts ensure stress reduction in the covering material during compression

First, it was necessary to pre-assemble the module without gluing, check the dimensions, and test the process of fixing the module BEFORE its final assembly. Based on the results from this stage, we can start the final gluing assembly of the module. Only three hours are available to complete this operation before the glue cure (Fig. 54).

Fig. 54. Gluing process; module, under a vacuum pressure of 26 tons; finished module in a box

After assembly, the CRV module and several strips were sent from JINR to the Georgian Technical University (GTU, Tbilisi) to conduct some bench tests of the CRV module and study the aging of the strips. The module was then delivered to KEK/J-Park (Japan) for preparation for the first cosmic muon tests using appropriate electronics and for their study during the COMET experiment Phase-α next year. Based on the results, a decision will be made regarding the serial production of these modules and the electronics. Before shipping, this module was first tested using the Meteor-32 Front-End electronics. Preliminary results showed that the calculated CRV efficiency of at least 99.99% was achieved in stationary conditions (Fig. 55).

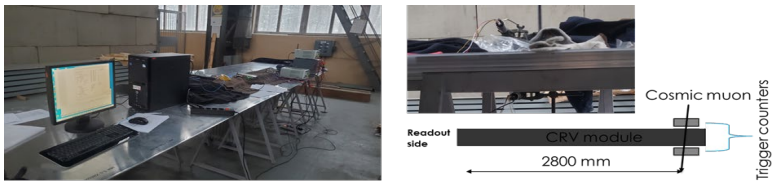

Fig. 55. The first tests of the CRV module with Meteor-32, conducted at JINR

We scheduled the first launch of the CRV module at J-PARC with Front-End electronics based on Meteor-32 because it is important to ensure that the calculated efficiency of the CRV (at least 99.99%) for detecting cosmic muons will be repeated in a natural environment with high neutron and gamma quantum fluxes.

Further, beginning in 2024, it will be necessary to start mass production of CRV strips, based on the experience gained from creating the first 100 strips, and ensure quality control of the strips to achieve a production rate of 128 strips/month. Front-Electronics must be produced at the same time. After producing the strips, they should be delivered to KEK to start the assembly of CRV modules and the mass production of FEBE in a local laboratory. Then, it is necessary to assemble the entire system and prepare it for the first commissioning run.

The results of all the research conducted were presented at the COMET collaboration meetings. Several publications describing these studies have also been scheduled in peer-reviewed journals.

2.2.6.5 Trigger systems

Phase-I will have two distinct running modes. One with the StrECAL as main detector to measure backgrounds and characterize the beam and the other with the CyDet as main detector to search for $\mu^-N \rightarrow e^-N$. There will be distinct but similar DAQ and trigger systems for the two modes. Detectors such as a beam monitor and an X-ray monitor (to determine the muon beam profile and number of muons captured in the target, respectively) will be employed for both modes. Similarly, the CRV will provide a veto whilst running with beam (which can be applied offline), but can also provide a calibration trigger.

The CyDet Trigger

The main trigger when operating in CyDet mode requires matches on neighboring hodoscope counters and tracks registered with the CDC, i.e. a 4-fold coincidence. The additional using of CDC signals is due to the fact that the signals of electrons with high momentum (signal or DIO) are completely different than for noise signals of particles with low momentum. For CyDet, a simple combination of the operation of the hodoscope counters and the energy contribution allows for a sufficiently fast launch with high background suppression efficiency, which leads to a total launch frequency of a few kHz.

StrECAL Trigger

The energy deposition from a single track can be divided among several crystals and so a summation is necessary to reconstruct the full energy. The sum of the energies in the crystals forming the 4×4 block is almost the entire energy deposited by an electron with an energy of about 100 MeV. The basic trigger unit (cell) will therefore be a group of 2×2 crystals (one ECAL crystal module), and the total energy will be determined by summing the total energy of the cells called the trigger group. The effectiveness from simulation shows at least a 10^6 DIO rejection for around a 90 % conversion electron detection efficiency.

A StrECAL cosmic trigger is also required for detector systems calibrations when not running with a beam. It will be based on the cosmic veto system with simple coincidences of hits in neighboring strips.

Trigger Rate

For the CyDet trigger the deadtime is less than 1 μs and hence the actual maximum trigger rate in CyDet mode is 440 kHz, whereas for the StrECAL trigger the deadtime is 36.7 μs that leading to a maximum trigger rate of 26 kHz. However, the effective trigger rate is dictated by the DAQ system, which is not greater than 20 kHz.

2.2.7 COMET Phase-α

Phase-α is planned to be implemented before Phase-I, in 2025. In Phase-α, it will be measured the kinematic parameters for each secondary particle, such as time and energy, as well as the proton beam itself. The yields are roughly 10^{-5} – 10^{-6} times as much as those in Phase-I, due to the limited geometrical acceptance. For particle identification (PID) simulation study it was used a combination of a plastic scintillator hodoscope and the ECAL. It was shown that e^- and most μ^- are clearly identified, while the PID efficiency for π^-, at less than 80% generally, requires further improvement.

In order to more precisely estimate the secondary beam yield and its characteristics, it will be carried out a mass production of simulation data with the new fully-detailed setup geometry.

Concerning the PID performance study: it was not taken into account the effects of particle decays between the detectors; the positions and dimensions of the detectors needed optimization to achieve higher statistics; hence, more algorithms should be examined for enhancing the PID performance, simulations with real detector parameters should be performed, and other possible detector combinations should be explored.

The following items, going beyond PID studies, are also considered. **First**, the ability of Phase-α to measure antiprotons is being investigated. Antiprotons are a potential source of backgrounds, but the production cross-section in the backwards direction is not well-understood. If this is measured to be small or cannot be seen in Phase-α (in this case it would be obtained an upper limit for antiproton production), this would represent an important milestone for the physics measurement in Phase-I. Now antiproton-producing physics models are implementing in COMET software - ICEDUST. **Second**, the detectors for measurements of the proton beam are also being developed at this time. **Third**, it is also planned to use a target made of aluminum in a setup that will allow to demonstrate the measurement of muonic X-rays. Lastly, it is possible to install a beam blocker in the detector region and assess its stopping power, because in the Phase-I beam measurement programme, it will be used to suppress the secondary beam flux before it reaches the detectors, and simulation work will be required to optimize the design of this component.

2.2.8 Simulation and Data Analysis

Development of the straw tracker and calorimeter systems required a lot of simulation work. The simulation of a straw tube with a diameter of 5 mm was performed using GARFIELD, and simulation of the plane geometry and evaluation of the detector accuracy was carried out using a special C++ program. The straw tube results (efficiency, spatial resolution) for Ar:CO_2 gas mixture (80:20) and 4×10^4 gas amplification are presented in Table 6 [31].

Table 6. Results of straw tube modeling

Diameter of straw tube [mm]	5	9.8
Max drift time [ns] stops/proton	38	120
Spatial resolution [μm]	83	73
Low efficiency region of track registration near the cathode [μm]	100	50
Rate capability	Depends on the type of front-end electronics	

Fig. 56 shows the R-T dependence for 5 mm straw tube, and Fig. 57 and Fig. 58 show the spatial resolution and integrated spatial resolution, respectively. A simulation of the optimal geometry of the straw tracker plane was performed, and the estimation of track reconstruction accuracy (better than 0.6 μm) was obtained (Fig. 59).

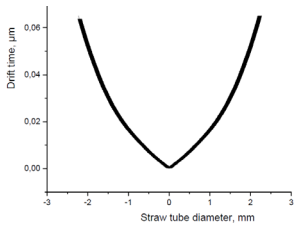

Fig. 56. Simulated R-T dependence for 5 mm straw tube

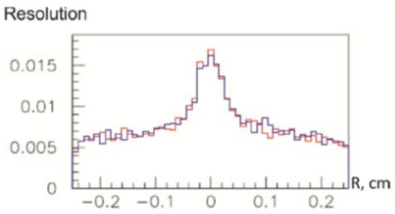

Fig. 57. Distribution of 5 mm straw tube spatial resolution over diameter

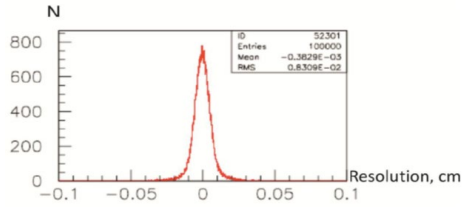

Fig. 58. Integral spatial resolution of 5 mm straw tube

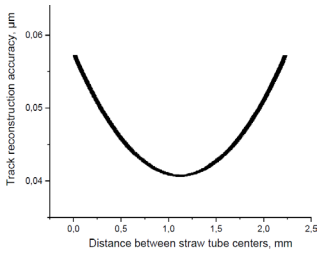

Fig. 59. Estimation of track reconstruction accuracy

A dedicated simulation has been done with the aim to optimize the operation of the J-PARC Main Ring in order to achieve very low extinction factor, below 10^{-9}, what is the must for COMET.

The Beam Test measurement data from the ECAL prototype obtained at the Tohoku electron accelerator were analyzed independently from the Japanese team. Based on the results of this analysis, it was concluded that the LYSO:Ce crystals parameters meet the requirements of the experiment better than GSO crystals. For the data analysis of the case where the electron beam incident angle was 20^{o} on the end surface of the prototype (on LYSO crystals) the energy resolution of 6.2% was obtained.

The Geant4 (G4) simulation of the optimal structure of the segmented calorimeter for the COMET experiment was made. Since the optical model of the LYSO crystal is not implemented in G4 package, it was developed using SLitrani package and measurements of the main optical parameters of the crystal performed by JINR specialists. To verify the G4 optical model, G4 simulation of the LYSO:Ce crystal was performed. Fig. 60 shows the simulated and measured energy spectra of the LYSO:Ce crystal, with both spectra superimposed for clarity.

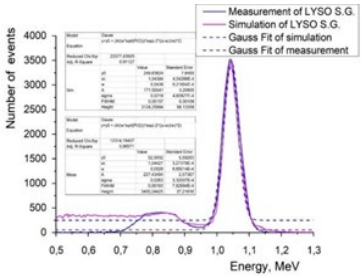

Fig. 60. Simulated and measured LYSO:Ce crystal energy spectra, obtained for the same conditions (APD, 22Na: 1274 keV, collimator opening 0.5 mm)

G4 simulations of the optimal ECAL structure were performed taking into account the crystal optical model and the real conditions of experiment, namely: ECAL was placed in a uniform magnetic field of 1 T; the spread of the electron beam was 10 ± 0.25 MeV, and ±1 cm in geometry; each crystal was wrapped with 2 layers of Teflon (60 μm).

The result of ECAL, consisted of LYSO:Ce crystals, simulation is shown in Fig. 61. The ECAL energy resolution (Fig. 61 (b)) was ~4.8%, which is in good agreement with the result of ~4.6% obtained in the Tohoku Beam Test measurements (Fig. 61 (c)) [32]. The simulation parameters of the ECAL prototype made of LYSO:Ce crystals are similar to the conditions under which the test measurements were carried out, with the exception of the magnetic field (it was not present during the measurements). Thus, the resulting G4 optical model can be used to simulate the ECAL and process the data from the COMET experiment [20, 29].

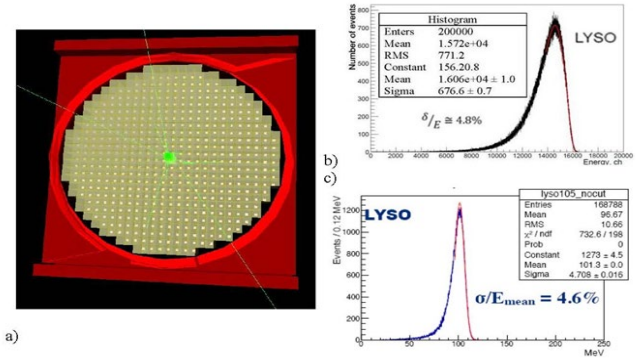

Fig. 61. Calorimeter simulation results: a) geometry b) detected energy spectrum; c) results of experimental measurement of the calorimeter prototype at the electron beam accelerator (2014, Tohoku)

A very important task is to work in the COMET software – ICEDUST, in particular, the optimal ECAL structure has been implemented, and work on simulation of the straw tracker response is underway.

In the future, we plan to expand our simulation and data analysis efforts to be ready for physical analysis of J-PARC's COMET data.

JINR's responsibility in the COMET experiment

- The JINR group is the only one within the COMET collaboration capable of producing thin-wall straw tubes, so we are **fully responsible** for their production. Various procedures have been updated to check tubes for pressure, gas leakage and elongation in accordance with COMET's requirements, and new testing standards have also been established.
- JINR takes **full responsibility** for the next step in this direction by carrying out R&D work on straw tubes for the COMET Phase-II, with a diameter of 5 mm and a wall thickness of 12 μm. For this purpose, we have prepared a new straw production line in DLNP.
- JINR physicists, together with KEK colleagues, take **full responsibility** for assembling, testing and installing the full-scale straw tracker for Phase-I. Appreciating JINR's crucial contribution to the creation of the straw tracker, the collaboration has elected a member of the JINR-COMET team to be one of the **coordinators for the straw tracker system.**
- JINR proposed the idea and took **full responsibility** for the production of a full-scale straw station for Phase-I, with a new type of straw tubes.
- JINR takes **full responsibility** for the development and optimization of the crystal calibration method for the calorimeter to be used in COMET Phase-I and Phase-II.
- JINR, together with KEK and Kyushu University, takes **full responsibility** for assembling, testing, installation and operation of the calorimeter.

- JINR physicists take **full responsibility** for crystal certification and are leaders in R&D work.
- JINR physicists implemented a full-scale R&D program to create a cosmic-ray veto system. The program was successfully completed, and the results were presented at collaboration meetings. Based on these results, all parameters and methods for creating the CRV were determined. Also, the **main responsibility** for the assembly, testing and installation of the CRV for Phase-I will be on JINR scientists. As a result, a member of the JINR group was elected **the COMET-CRV leader**.

The plans for 2025-2029 include

- Participation in the preparation, engineering and physics run, the data acquisition and analysis of Phase-I, 2025-2027.
- Simulation of a complex detector system (tracker, calorimeter, etc.), 2025-2027.
- R&D program for the production of straw tubes with a wall thickness of 12 μm and a diameter of 5 mm. Measurement of all mechanical properties and development of quality control standards for manufactured new straw tubes of diameter 5 mm, 2025.
- Completion of assembly, testing, calibration, installation, cosmic test and maintenance of the straw detector for Phase-I, 2025-2026.
- Production of straw tubes (about 1000 pcs) for a full-scale prototype, 2026-2027.
- Production of a full-scale straw station at JINR, with new tubes (12 μm, 5 mm), and measurements on the beam, 2027-2028.
- Preparation, mass-production and testing of straw tubes for Phase-II, 2028-2029.
- Development and optimization of the crystal calibration method for the COMET calorimeter, considering the features of the experiment: the presence of magnetic field and high-resolution calorimeter, 2025-2026.
- Participation in the design, assembly, installation, cosmic test and maintenance of the calorimeter in full, 2025-2027.
- Participation in the assembly and maintenance of the CRV for Phase-I and Phase-II, 2025-2029.
- Participation in the beam tests of detector components for Phase-II, 2028-2029.
- Participation in the assembly, testing, installation and maintenance of the entire detector system for Phase-II, 2028-2029.

The publications and reports at conferences by JINR-COMET group

Publications

1. V. Kalinnikov, Velicheva and A. Rozhdestvensky, “Measurement of the LYSO:Ce and LYSO:Ce,Ca scintillator response for the electromagnetic calorimeter of the COMET experiment” / Physics of Particles and Nuclei Letters, 2023, Vol. 20, No. 5, pp. 995–1001.

2. A. Artikov, V. Baranov, A. Boikov, D. Chokheli, Yu.I. Davydov, V. Glagolev, A. Simonenko, Z. Tsamalaidze, I. Vasilyev, I. Zimin. High efficiency muon registration system based on scintillator strips. // Physics > Instrumentation and Detectors: arXiv:2309.14515, 2023.

3. V. Kalinnikov, E. Velicheva, Measurement of the Electromagnetic Calorimeter Prototype using Cosmic Muons // Physics of Particles and Nuclei Letters, 2022, Vol. 19, No. 3, pp. 225–234. © Pleiades Publishing, Ltd., 2022.

4. V. Kalinnikov, E. Velicheva, Yusuke Uozumi, Comparison of the Scintillation Properties of Long LYSO:Ce Crystals from Different Manufacturers. //Physics of Particles and Nuclei Letters, 2021, Vol. 18, No. 4, pp. 457–468.

5. A. Volkov*, P. Evtoukhovich, M. Kravchenko, Y. Kuno, S. Mihara, H. Nishiguchi, A. Pavlov, Z. Tsamalaidze. Properties of straw 1 tubes for the tracking detector of the COMET experiment.// NIM, A, Volume 1004, article id. 165242, 2021.
6. H. Nishiguchi, P. Evtoukhovitch, Y. Fujii, E. Hamada, N. Kamei, S. Mihara, A. Moiseenko, K. Noguchi, K. Oishi, J. Suzuki, J. Tojo, Z. Tsamalaidze, N. Tsverava, K. Ueno, A. Volkov, Construction on vacuum-compatible straw tracker for COMET Phase-I. NIM, A 958 (2020) 162800.
7. Kalinnikov et. al, Investigation of the light yield distribution in LYSO crystal by the optical spectroscopy method for the electromagnetic calorimeter of the COMET experiment // Nonlinear Phenomena in Complex Systems, vol. 23, no. 4 (2020), pp. 374 – 385.
8. А. Д. Волков, М. Д. Кравченко, А. В. Павлов. Стенд для исследования характеристик строу. Успехи прикладной физики, 2019, том 7, № 1, стр. 76 - 83.
9. А. Д. Волков, П. Г. Евтухович, А. С. Моисеенко, Б. М. Сабиров, З. Цамалаидзе, Н. Цверава. Влияние внутреннего давления на натяжение в сварных строу трекового детектора. Успехи прикладной физики, 2018, том 6, № 1, стр. 83 – 90.
10. А. Д. Волков, М. Д. Кравченко, А. В. Павлов. Устройство для исследования свойств строу трубки координатного детектора частиц. Патент № 2691770.
11. H. Nishiguchi, P. Evtoukhovitch, A. Moiseenko, Z. Tsamalaidze, N. Tsverava, A. Volkov, et al. Development of an extremely thin-wall straw tracker operational in vacuum- The COMET straw tracker system. NIM, A 845, 269 (2017).
12. В. Калинников, Е. Величева, З. Цамалаидзе, А. Лобко, О. Мисевич, Исследование методов улучшения однородности светосбора в кристаллах для электромагнитного калориметра эксперимента «COMET»// Сб.: Аспекты сцинтилляционной техники. (под редакцией А.В. Гектина) – Харьков: “ИСМА”, 2017. С.21-41 с.
13. А. Д. Волков, З. Цамалаидзе. Способ определения коэффициента Пуассона материала герметичной тонкостенной полимерной трубки. Патент № 2653186.
14. COMET Phase-I. Technical Design Report 2016 (prepared with participation of the JINR physicists).
15. V. Kalinnikov, E. Velicheva, Z. Tsamalaidze, Lobko, O. Missevitch, Y. Kuno. Spatial and temporal evolution of scintillation light in LYSO electromagnetic calorimeter for non-paraxial electromagnetic showers. //Nonlinear Phenomena in Complex. V. 19, No 4 (2016). Pp. 345 – 357.
16. V. Kalinnikov, E. Velicheva. Research of the ECAL calorimeter used in the COMET experiment. // Functional Materials, 22 (2015), 1, 116-125.
17. V. Kalinnikov, E. Velicheva. Research of long GSO and LYSO crystals used in the calorimeter developed for the COMET experiment. Functional Materials, 22 (2015), 1, 126-134.
18. V. Kalinnikov, E. Velicheva. Simulation of Long GSO Crystals for the COMET Experiment. // Nonlinear Phenomena in Complex. V. 8, No 2 (2015). Pp. 215 – 221.
19. В. Калинников, Е. Величева, А. Лобко. Исследование длинных кристаллов GSO и LYSO для создания сегментированных электромагнитных калориметров. Физика сцинтилляторов. Материалы, методы, аппаратура. Изд: ИСМА. 2015. С. 137-158.
20. Калинников В., Величева Е. Исследование параметров и разработка алгоритма пространственной реконструкции для калориметра COMET эксперимента. Изд: ИСМА. 2015. С. 186-203.
21. V. Kalinnikov, E. Velicheva. Investigation of LYSO and GSO crystals and simulation of the calorimeter for the COMET experiment. // Phys. Part. Nucl. Lett. 11 (2014) 3, 259-268.
22. M. Eliashvili, A. Khvedelidzre, M. Nioradze, Z. Tsamalaidze. The COMET experiment at J-PARC: A step towards solving the muon enigma, TSU Science, N6, (2014).

23. А.Д. Волков. Контроль натяжения трубок в строу детекторах. Успехи прикладной физики, 2, №4, 413 (2014).
24. V. Kalinnikov, E. Velicheva, The Calorimeter Simulation. Comet Technical Note 108_V1.2014.
25. A.D. Volkov. Wire tension monitor for proportional chambers of the ANKE spectrometer. NIM A 701, 80 (2013).
26. А.Д. Волков. Устройство для измерения натяжения трубки в строу детекторах. Патент №2539107 (2013).
27. V. Kalinnikov, E. Velicheva, The Calorimeter Simulation. Comet Technical Note 26_V1.2012.

Reports at conferences

1. N. Tsverava, D. Chokheli et al, “JINR/GTU straw laboratory current activity”, COMET Collaboration meeting 42 (CM42), Zoom J-PARC, Japan, Feb 2024
2. D. Chokheli, Z. Tsamalaidze, “Schedule to work with 1st CRV module and next plan for mass production”, COMET Collaboration meeting 42 (CM42), Zoom J-PARC, Japan, Feb 2024
3. D. Chokheli, “Some info about 1st CRV module: preparation”, COMET Collaboration meeting 41 (CM41), Zoom J-PARC, Japan, Nov 2023
4. D. Chokheli, “Summary of CRV status”, COMET Collaboration meeting 41 (CM41), Zoom J-PARC, Japan, Nov 2023
5. D. Chokheli, Z. Tsamalaidze, “First CRV-Left module status and plan for coming autumn”, COMET Collaboration meeting 40 (CM40), Zoom J-PARC, Japan, July 2023
6. P. G. Evtoukhovitch, Samartsev A., Pavlov A., Tsamalaidze Z., Tsverava N. et al, “Production of some components for 5mm straw module: status and perspectives”, COMET Collaboration meeting 39 (CM39), Zoom J-PARC, Japan, Mar 2023
7. D. Chokheli et al, “The CRV module, preliminary test with Meteor32, processing to send it to KEK”, COMET Collaboration meeting 39 (CM39), Zoom J-PARC, Japan, Mar 2023
8. D. Chokheli et al, “Straw chambers array as a temporary/backup solution for CRV front area for Phase-1”, COMET Collaboration meeting 39 (CM39), Zoom J-PARC, Japan, Mar 2023
9. D. Chokheli et al, “Summary of CRV status”, COMET Collaboration meeting 39 (CM39), Zoom J-PARC, Japan, Mar 2023
10. D. Chokheli, Z. Tsamalaidze, “COMET CRV STATUS for CM38”, COMET Collaboration meeting 38 (CM38), Zoom J-PARC, Japan, Dec 2022
11. D. Chokheli et al, “Front-end electronics for CRV: design of version 1.0 is ready for discussion”, COMET Collaboration meeting 38 (CM38), Zoom J-PARC, Japan, Dec 2022
12. D. Chokheli et al, “Creation of COMET CRV Module CRV-SL-0”, COMET Collaboration meeting 38 (CM38), Zoom J-PARC, Japan, Dec 2022
13. D. Chokheli, Z. Tsamalaidze, “COMET CRV STATUS for CM37”, COMET Collaboration meeting 37 (CM37), Zoom J-PARC, Japan, July 2022
14. D. Chokheli et al, “Creation of COMET CRV Module CRV-SL-0”, COMET Collaboration meeting 37 (CM37), Zoom J-PARC, Japan, July 2022
15. N. Tsverava, “Status Report on 12μm Straw”, COMET Collaboration meeting 37 (CM37), J-PARC, Japan, Jul 2022
16. P. G. Evtoukhovitch et al, “Production and testing the ROESTI slightly modified”, COMET Collaboration meeting 37 (CM37), Zoom J-PARC, Japan, Jul 2022
17. D. Chokheli, “COMET CRV STATUS for CM36”, COMET Collaboration meeting 36 (CM36), Zoom J-PARC, Japan, Mar 2022

18. D. Chokheli et al, “Starting a creation of the 1st COMET CRV Module “0””, COMET Collaboration meeting 36 (CM36), Zoom J-PARC, Japan, Mar 2022
19. A. Boikov, D. Chokheli et al, “DAQ for the quality test while mass production and first steps with PETIROC”, COMET Collaboration meeting 36 (CM36), Zoom J-PARC, Japan, Mar 2022
20. D. Chokheli et al, “Scintillator CRV: getting ready for mass production”, COMET Collaboration meeting 36 (CM36), Zoom J-PARC, Japan, Mar 2022
21. A. Boikov, D. Chokheli et al, “DAQ for the quality test while mass production and first steps with PETIROC”, COMET Collaboration meeting 35 (CM35), Zoom J-PARC, Japan, Nov 2021
22. D. Chokheli et al, “Scintillator CRV: getting ready for mass production”, COMET Collaboration meeting 35 (CM35), Zoom J-PARC, Japan, Nov 2021
23. D. Chokheli, “COMET CRV STATUS for CM35”, COMET Collaboration meeting 35 (CM35), Zoom J-PARC, Japan, Nov 2021
24. D. Chokheli et al, “CRV draft design for side and top”, COMET Collaboration meeting 33 (CM34), Zoom J-PARC, Japan, July 2021
25. A. Boikov, D. Chokheli et al, “R&D for COMET CRV Front End Board electronics: some tests with CITIROC and LiROC”, COMET Collaboration meeting 34 (CM34), Zoom J-PARC, Japan, July 2021
26. D. Chokheli, I. Zimin et al, “Background estimation for module: reflection from the back wall, rate for the electrons, neutrons, gammas”, COMET Collaboration meeting 34 (CM34), Zoom J-PARC, Japan, July 2021
27. D. Chokheli. “R&D for CRV system based on scintillator strips for the COMET experiment”, CM33 workshop, Tokai, J-PARC, 22 February to 4 March, 2021
28. E. Kaneva. “SimG4 Bug: Pion Production Region Geometry”, CM32, Zoom J-PARC, 2-6 November, 2020
29. D. Chokheli. “ High Efficiency Muon Registration System based on Scintillator Strips”, CM32 workshop, Tokai, 2-6 November, 2020
30. S. Tereshchenko. “ Proposal for Improvement of the efficiency and electronic for the CRV”, CM32 workshop, Tokai, J-PARC, 2-6 November, 2020
31. N. Tsverava et al., “Development of Ultrathin 12 μm Thick Straw Tubes for the Tracking Detector of COMET Experiment”, Proceedings, 2019 IEEE Nuclear Science Symposium (NSS) and Medical Imaging Conference (MIC) (NSS/MIC 2019): Manchester, United Kingdom, October 26 - November 02, 2019
32. N. Tsverava. “Examination the quality of the seams of 12/20 μm straw tubes”, CM29 workshop, Tokai, J-PARC, 14-18 Oct, 2019
33. V. Duginov. “The certification of the LYSO(Ce) crystals for COMET calorimeter”, The COMET colloquium, Dubna, October 2019
34. M. Kravchenko. “Mechanical properties of the thin-walled straws of the COMET experiment”, The EPS-HEP2019 Conference, Ghent, Belgium, 10-17 July, 2019
35. N. Tsverava. “Straw tubes R&D for Phase-II”, CM28 workshop, Tokai, 10-14 June, 2019
36. A. Pavlov. “The first step in obtaining a three-dimensional drift line”, CM27 workshop, Tokai, 19-23 Feb, 2019
37. A. Pavlov, P. Evtoukhovitch. “The final result of simulation of the drift line in Garfield ++”, CM28 workshop, Tokai, 19-23 Feb, 2019
38. A. Pavlov., P. Evtoukhovitch. “The simplify model of electron drifting in the straw tube”, CM27 workshop, Tokai, 19-23 Feb, 2019

39. P. Evtoukhovitch. “New steps in the straw module development for 5 mm straws”, CM27 workshop, Tokai, 19-23 Feb, 2019
40. H. Nishiguchi, P. Evtoukhovitch, et al., “Construction on vacuum-compatible straw tracker for COMET Phase-I”, The 15th Vienna Conference on Instrumentation, Vienna, Austria, February 18-22, 2019
41. V. Duginov. “The pasportization of the LYSO(Ce) crystals for COMET”, the COMET CM26 workshop, Tbilisi, 1-5 October 2018
42. A. Pavlov. “Simulation of drift lines. The nature of the electron motion in the tube”, CM26 workshop, Tbilisi, 1-5 Oct, 2018
43. M. Kravchenko, A. Pavlov. “Mechanical properties of the thin-walled welded straws for the COMET experiment”, CM26 workshop, Tbilisi, 1-5 Oct, 2018
44. A. Pavlov. “The effect of the seam on the collection of primary ionization”, European School of High-Energy Physics, Maratea, Italy, 20 June – 3 July, 2018
45. A. Pavlov. “The effect of the gap on the collection of primary ionization”, CM25 workshop, Tokai, 21-25 May, 2018
46. P.Evtoukhovitch. “Present status of the straw module prototype with 5 mm straws”, CM25 workshop, Tokai, 21-25 May, 2018
47. A. Pavlov, P. Evtoukhovitch. “Position Resolution of the Straw Tube”, CM23 workshop, TU-Dresden, 24-30 Sep, 2017
48. K. Ueno, P. Evtoukhovitch, et al., “Development of a thin-wall straw-tube tracker for COMET experiment”, Proceedings, 2017 European Physical Society Conference on High Energy Physics (EPS-HEP 2017): Venice, Italy, July 5-12, 2017
49. Z. Tsamalaidze. “The status and plans of JINR activity in the COMET experiment”, the COMET CM22 workshop, Tokai, 29 May – 02 June, 2017
50. E. Velicheva, V. Kalinnikov. “Simulation and Experimental Investigation of Optical Properties of Inorganic Crystals”, BelINP-2017, 1st International Symposium “Integration of Belarasion Scientists in the reseach programs of the world’s leading nuclear physics centers”. May 2017

References

1. The COMET Collaboration, Conceptual design report for experimental search for lepton flavor violating $\mu^- \rightarrow e^-$ conversion at a sensitivity of 10^{-16} with a slow-extracted bunched proton beam (COMET), KEK Report 2009–10 (submitted to the J-PARC Physics Advisory Committee) (2009) (available at: https://lib-extopc.kek.jp/preprints/PDF/2009/0924/0924011.pdf).
2. COMET Phase-I TDR, COMET Collaboration, PTEP 2020, 3, 033C01.
3. B. Krikler, Sensitivity and background estimates for Phase-II of the COMET experiment, Ph.D. Thesis, Imperial College London (2016).
4. W. Bertl et al., Eur. Phys. J. C 47, 337 (2006).
5. R.M. Carey et al.,"Proposal to Search for $\mu^-N \rightarrow e^-N$ with a Single Event Sensitivity Below 10^{-16}", FERMILAB-PROPOSAL-0973.
6. E. Oset, H. C. Chiang, T. S. Kosmas, A. Faessler, and J. D. Vergados, 13th Int. Conf. Particles and Nuclei (PANIC 93), p. 271 (1993).
7. D. Tomono et al., Proc. 2017 Int. Workshop on Neutrinos from Accelerators (NuFact17), p. 111 (2018).
8. H. Sakamoto, Simulation Studies for the CDC for COMET Phase-I, COMET internal note No. 34 (2013).
9. S. Movchan, Nucl. Instrum. Meth. A 604, 307 (2009).

10. A. Volkov, P. Evtoukhovich, M. Kravchenko, Y. Kuno, S. Mihara, H. Nishiguchi, A. Pavlov, Z. Tsamalaidze // Properties of straw tubes for the tracking detector of the COMET experiment, Nuclear Instruments and Methods in Physics Research Section A: Accelerators, Spectrometers, Detectors and Associated Equipment, Volume 1004, 11 July 2021, 165242, https://doi.org/10.1016/j.nima.2021.165242
11. А. Д. Волков, М. Д. Кравченко, А. В. Павлов. Устройство для исследования свойств строу трубки координатного детектора частиц. Патент № 2691770.
12. Mendelson A. Plasticity: Theory and Application. New York: Macmillan, 1968
13. Birger I.A., Mavlyutov R.R., Resistance of Materials. Moskow: Nauka, 1986
14. http://www.detectors.saint-gobain.com/
15. C. Pepin, et.al. Properties of LYSO and recent LSO scintillators for phoswich PET detectors. IEEE Trans. Nucl. Sci., vol. 51, No. 3, (2004) pp. 789-795.
16. Weber S, Christ D, Kurzeja M et al. (2003) Comparison of LuYAP, LSO, and BGO as scintillators for high resolution PET detectors. IEEE Trans. Nucl. Sci. 50: 1370–1372.
17. Carelhtt W.E. vanEijk. Inorganic scintillators in medical imaging detectors, Nuclear Instruments and Methods in Physics Research A 509 (2003) 17-25.
18. Cordelli M. et al., Test of a LYSO matrix with an electron beam between100 and 500 MeV for KLOE-2 // Nuclear Instruments and Methods in Physics Research A 617 (2010) 109–112.
19. C. Fabjan, F. Gianotti. Calorimetry for particle physics. Published in Rev.Mod.Phys. 75 (2003) 1243-1286.
20. V. Kalinnikov, E. Velicheva, Y. Kuno et al. Spatial and temporal evolution of scintillation light in LYSO electromagnetic calorimeter for non - paraxial electromagnetic showers. //Nonlinear Phenomena in Complex. V. 19, No 4 (2016). Pp. 345.
21. Hans-Christian Schultz-Coulon. The Physics of Particle Detectors. Lecture& Journal Club (SS 2011). Kirchhoff-Institut für Physik. http://www.kip.uni-heidelberg.de/~coulon/Lectures/Detectors/Free_PDFs/Lecture9.pdf
22. https://www.caen.it/sections/digitizer-families/
23. https://www.hamamatsu.com/resources/pdf/etd/High_energy_PMT_TPMZ0003E.pdf
24. V. Kalinnikov, E. Velicheva, Measurement of LYSO crystals. Comet Technical Note 107_V1.2014.
25. V. Kalinnikov, E. Velicheva. Investigation of LYSO and GSO crystals and simulation of the calorimeter for the COMET experiment. // Phys. Part. Nucl. Lett. 11 (2014) 3, 259-268.
26. V. Kalinnikov, E. Velicheva, Yusuke Uozumi, Comparison of the Scintillation Properties of Long LYSO:Ce Crystals from Different Manufacturers. //Physics of Particles and Nuclei Letters, 2021, Vol. 18, No. 4, pp. 457–468).
27. В. Калинников, Е. Величева, З. Цамалаидзе, А. Лобко, О. Мисевич, Исследование методов улучшения однородности светосбора в кристаллах для электромагнитного калориметра эксперимента «COMET»// Сб.: Аспекты сцинтилляционной техники. (под редакцией А.В. Гектина) – Харьков: “ИСМА”, 2017. С.21-41.
28. V. Kalinnikov, E. Velicheva, Measurement of the Electromagnetic Calorimeter Prototype using Cosmic Muons // Physics of Particles and Nuclei Letters, 2022, Vol. 19, No. 3, pp. 225–234. © Pleiades Publishing, Ltd., 2022.
29. V. Kalinnikov, Velicheva and A. Rozhdestvensky, “Measurement of the LYSO:Ce and LYSO:Ce,Ca scintillator response for the electromagnetic calorimeter of the COMET experiment” / Physics of Particles and Nuclei Letters, 2023, Vol. 20, No. 5, pp. 995–1001.
30. https://pdf.directindustry.com/pdf/hamamatsu/si-apd/13622-597330.html

31. V. Kalinnikov, E. Velicheva, The simulation of the COMET straw tracker. Comet Technical Note 36_V1_2013.
32. Kou Oishi, Development of Electromagnetic Calorimeter Using LYSO Crystals for the COMET Experiment at J-PARC, Published in: PoS EPS-HEP2017 (2018) 800.

2.3 Estimated completion date

2025 - 2029

2.4 Participating JINR laboratories

DLNP, VBLHEP, BLTP, MLIT

2.4.1 MICC resource requirements

Computing resources	**Distribution by year**				
	1st year	2nd year	3rd year	4th year	5th year
Data storage (TB) - EOS - Tapes					
Tier 1 (CPU core hours)					
Tier 2 (CPU core hours)					
SC Govorun (CPU core hours) - CPU - GPU					
Clouds (CPU cores)					

2.5. Participating countries, scientific and educational organizations

Organization	**Country**	**City**	**Participants**	**Type of agreement**
Imp. college Rutherf. Lab.	England	London	Uchida Yoshi + 6 pers. Clark D. + 4 pers.	Joint work
IF NANB	Belarus	Minsk	Shelkovyi D.V. + 3 pers. Orlovich V, Grabchikov A, Khodasevich I	Joint work
BGU	Belarus	Minsk	Anishchik V.M. + 5 pers.	Joint work
INR, BGU	Belarus	Minsk	Lobko A., Misevich O.	Joint work
Tech. Univ	Germany	Dresden	Zuber K. + 4 pers.	Joint work
IHEP-TSU	Georgia	Tbilisi	Devidze G. + 4 pers.	Joint work
GTU	Georgia	Tbilisi	Lomidze D. + 6 pers.	Joint work
UG	Georgia	Tbilisi	Gogilidze + 2 pers.	Joint work
INP ME	Kazakhstan	Almaty	Zdorovets M.+3 pers.	Joint work
BINP RAS	Russia	Novosibirsk	Grigoriev D. + 6 pers.	Joint work

NSU	Russia	Novosibirsk	Bondar A. + 6 pers.	Joint work
CNRS-IN2P3	France	Paris	Kapusta F. + 4 pers.	Joint work
Karlov Univ.	Czech Republic	Prague	Finger M. + 4 pers.	Joint work
KEK	Japan	Tsukuba	Mihara S. + 18 pers.	Joint work
Osaka Univ.	Japan	Osaka	Kuno Y. + 14 pers.	Joint work
Kyushu Univ.	Japan	Fukuoka	J. Tojo + 8 pers.	Joint work

2.6. Key partners *(those collaborators whose financial, infrastructural participation is substantial for the implementation of the research program. An example is JINR's participation in the LHC experiments at CERN)*

3. Manpower

3.1. Manpower needs in the first year of implementation

№№ n/a	**Category of personnel**	**JINR staff, amount of FTE**	**JINR Associated Personnel, amount of FTE**
1.	research scientists	11.3	5
2.	engineers	3.1	
3.	specialists		
4.	office workers		
5.	technicians		
	Total:	**14.4**	**5**

3.2. Available manpower

3.2.1. JINR staff

No.	**Category of personnel**	**Full name**	**Division**	**Position**	**Amount of FTE**
1.	research scientists	D. Aznabaev	BLTP	Researcher	0.2
2.	research scientists	D. Baigarashev	VBLHEP	Researcher	0.2
3.	research scientists	D.Chokheli	DLNP	Senior researcher	1.0
4.	research scientists	T.L. Enik	VBLHEP	Senior researcher	0.1
5.	research scientists	D. Goderidze	MLIT	Junior researcher	0.4
6.	research scientists	P.G. Evtukhovich	DLNP	Senior researcher	1.0
7.	research scientists	A. Issadikov	BLTP	Senior researcher	0.2
8.	research scientists	V.A. Kalinnikov	DLNP	Leading researcher	1.0

9.	research scientists	A. Khvedelidze	MLIT	Leading researcher	0.4
10.	research scientists	G.A. Kozlov	BLTP	Leading researcher	0.2
11.	research scientists	A.V. Pavlov	DLNP	Junior researcher	1.0
12.	research scientists	B.M. Sabirov	DLNP	Researcher	1.0
13.	research scientists	A.V. Simonenko	DLNP	Senior researcher	0.5
14.	research scientists	V.V. Tereshchenko	DLNP	Group Leader	0.1
15.	research scientists	Z. Tsamalaidze	DLNP	Head of the Sector	0.7
16.	research scientists	N. Tsverava	DLNP	Junior researcher	1.0
17.	research scientists	I.I. Vasiliev	DLNP	Junior research	0.3
18.	research scientists	E.P. Velicheva	DLNP	Senior researcher	1.0
19.	research scientists	A.D. Volkov	DLNP	Researcher	1.0
20.	engineers	I.L. Evtukhovich	DLNP	Senior engineer	0.9
21.	engineers	E.S. Kaneva	DLNP	Engineer	1.0
22.	engineers	X. Khubashvili	DLNP	Engineer	0.9
23.	engineers	A.G. Samartsev	DLNP	Senior engineer	0.3
24.	specialists				
25.	technicians				
	Total:				**14.4**

3.2.2. JINR associated personnel

No.	**Category of personnel**	**Partner organization**	**Amount of FTE**
1.	research scientists		5
2.	engineers		
3.	specialists		
4.	technicians		
	Total:		**5**

4. Financing

4.1 Total estimated cost of the project/LRIP subproject

The total cost estimate of the project (for the whole period, excluding salary).
990000 USD
The details are given in a separate table below.

4.2 Extra funding sources

Expected funding from partners/customers – a total estimate.

Project Leader _____/__Tsamalaidze Zviadi_ _/

Date of submission of the project to the Chief Scientific Secretary: _____
Date of decision of the laboratory's STC: _20.03.2024___ document number: _____
Year of the project start: _____2021_____
(for extended projects) – Project start year: ___2015____

Proposed schedule and resource request for the Project

Expenditures, resources, funding sources			Cost (thousands of US dollars)/ Resource requirements	Cost/Resources, distribution by years				
				1st year	2nd year	3rd year	4th year	5th year
		International cooperation	600	120	120	120	120	120
		Materials	220	80	80	20	20	20
		Equipment, Third-party company services	170	40	40	30	30	30
		Commissioning						
		R&D contracts with other research organizations						
		Software purchasing						
		Design/construction						
		Service costs (*planned in case of direct project affiliation)*						
Resources required	**Standard hours**	Resources						
		– the amount of FTE,						
		– accelerator/installation,	1300	350	350	200	200	200
		– reactor,…						
Sources of funding	**JINR Budget**	JINR budget *(budget items)*	990	240	240	170	170	170
	Extra fudning (supplementary estimates)	Contributions by partners Funds under contracts with customers Other sources of funding						

Project (LRIP subproject) Leader _____/__Tsamalaidze Zviadi___/

Laboratory Economist _____/_____/

APPROVAL SHEET FOR PROJECT / LRIP SUBPROJECT

TITLE OF THE PROJECT / LRIP SUBPROJECT

SHORT DESIGNATION OF THE PROJECT **COMET**

PROJECT/LRIP SUBPROJECT CODE

THEME CODE 02-2-1144-2021

NAME OF THE PROJECT LEADER Tsamalaidze Zviadi

AGREED

JINR VICE-DIRECTOR	SIGNATURE	NAME	DATE
CHIEF SCIENTIFIC SECRETARY	SIGNATURE	NAME	DATE
CHIEF ENGINEER	SIGNATURE	NAME	DATE
LABORATORY DIRECTOR	SIGNATURE	NAME	DATE
CHIEF LABORATORY ENGINEER	SIGNATURE	NAME	DATE
LABORATORY SCIENTIFIC SECRETARY THEME / LRIP LEADER	SIGNATURE	NAME	DATE
PROJECT / LRIP SUBPROJECT LEADER	SIGNATURE	NAME	DATE

APPROVED BY THE PAC

SIGNATURE	NAME	DATE